ELSEVIER

Engineering Analysis with Boundary Elements ▮ (▮▮▮▮) ▮▮▮–▮▮▮

ENGINEERING ANALYSIS with BOUNDARY ELEMENTS

www.elsevier.com/locate/enganabound

The plane wave method for inverse problems associated with Helmholtz-type equations

Bangti Jin[a], Liviu Marin[b,*]

[a]Department of Mathematics, The Chinese University of HongKong, Shatin N.T., Hong Kong, PR China
[b]School of Mechanical, Materials and Manufacturing Engineering, The University of Nottingham, University Park, Nottingham NG7 2RD, UK

Received 16 March 2007; accepted 13 August 2007

Abstract

In this paper, a numerical scheme based on the meshfree plane wave method applied to inverse boundary value problems associated with Helmholtz-type equations is investigated. The resulting ill-conditioned system of linear algebraic equations is solved in a stable manner by employing the truncated singular value decomposition, while the optimal truncation number, i.e. the regularization parameter, is determined using the *L*-curve criterion. Numerical results are presented for two- and three-dimensional problems in smooth and piecewise smooth geometries, with both exact and noisy data. The accuracy, convergence and stability of the numerical method are analysed and, furthermore, a comparison with other meshless methods is also performed.

Keywords: Inverse problems; Helmholtz-type equations; Plane wave method; Ridge function; Meshfree/meshless method; Regularization

1. Introduction

Helmholtz-type equations arise in various scientific and engineering problems related to wave phenomena. They are frequently used for analysing acoustics, wave scattering, vibration of membranes and other structures and electromagnetic field. Another important application of Helmholtz-type equations is heat conduction in a fin [1]. The knowledge of the boundary conditions on the entire boundary of the solution domain gives rise to forward problems for Helmholtz-type equations, which have been extensively studied both mathematically and numerically [2–7].

However, many engineering applications of practical importance lead to inverse problems for Helmholtz-type equations. In particular, the boundary conditions are often incomplete due to technical difficulties with data acquisition. For example, a part of the boundary is inaccessible to direct measurements and the presence of measuring devices would disturb the physical process under investigation. These inverse problems are often ill-posed, in the sense that a small perturbation in the data could cause an enormous deviation of the solution. A classical example for an inverse problem associated with Helmholtz-type equations is the Cauchy problem. For details on its practical applications and relevant theoretical results, we refer the reader to Refs. [8–11].

Several numerical methods have been proposed for solving the Cauchy problem associated with Helmholtz-type equations [10–27]. Roughly speaking, these methods can be divided into direct and iterative methods. Direct methods usually employ regularization methods, such as the Tikhonov regularization method and the singular value decomposition (SVD), to stabilize the problem. Reginska and Reginska [10] studied the reconstruction of radiation field using regularization in the frequency domain. Bai [12] proposed a boundary element method (BEM) based acoustic holography technique employing the SVD for reconstructing sound fields. Wang and Wu [13] and Wu and Yu [14] developed the Helmholtz equation least-squares (HELS) method based on the spherical wave expansion for reconstructing acoustic pressure fields, whilst

*Corresponding author. Tel.: +44 115 846 7683; fax: +44 115 951 3800.
E-mail addresses: kimbtsing@yahoo.com.cn (B. Jin), liviu.marin@nottingham.ac.uk (L. Marin).

0955-7997/$ - see front matter © 2007 Elsevier Ltd. All rights reserved.
doi:10.1016/j.enganabound.2007.08.005

Isakov and Wu [15] provided a mathematical justification for it. Recently, Semenova and Wu [16] compared three expansions in the HELS method, namely the localized spherical waves, distributed spherical waves and distributed point sources. DeLillo et al. [17] formulated an integral equation approach to detect the source of acoustical noise inside the cabin from measurements of the acoustical pressure field. The marching scheme has been applied to the Helmholtz equation by Knightly and St. Mary [11] and Natterer and Wübbeling [18], whilst its convergence has recently been analysed by Natterer and Wübbeling [19]. However, the application of the marching scheme to irregular domains seems to be not straightforward. Recently, two methods based on the boundary knot method (BKM) and the method of fundamental solutions (MFS) have been proposed for the efficient solution of inverse problems for Helmholtz-type equations, see Jin and Zheng [20,21], Marin and Lesnic [22], Marin [23] and Wei et al. [24].

In the case of iterative methods, one starts with an initial guess for the unknown boundary condition and adjusts it iteratively by minimizing a certain functional, such as the L^2-norm of the error between the predicted system response and experimentally observed data. This approach could be computationally expensive since each iteration requires several forward solvers and many iterations may be required to get an accurate approximation. Marin et al. [25,26] have solved the Cauchy problem for Helmholtz-type equations by employing the BEM, in conjunction with an alternating iterative algorithm originally introduced by Kozlov et al. [28] and the conjugate gradient method (CGM), respectively. A preliminary comparison between direct and iterative methods applied to solving the Cauchy problem for Helmholtz-type equations has also been undertaken by Marin et al. [27].

In the present paper, we propose a novel meshless numerical scheme based on the plane wave method (PWM), in conjunction with the truncated SVD (TSVD), for solving inverse problems associated with Helmholtz-type equations directly. The outline of the paper is as follows. In Section 2, we formulate the problem mathematically. The following section is devoted to the proposed numerical scheme: The PWM for discretizing Helmholtz-type equations and regularization techniques for solving ill-conditioned systems of linear algebraic equations. In Section 4, we present numerical results obtained for several examples in two- and three-dimensional domains with both smooth and piecewise smooth geometries. Finally, concluding remarks are given in Section 5.

2. Mathematical formulation of the problem

Let Ω be an open simply connected bounded domain in $\mathbb{R}^d$, where d is the dimension of the space, and $\Gamma = \partial\Omega$ its boundary. Then the mathematical formulation of the problem in the absence of source terms is given by

$$(\Delta + \kappa^2)u(\mathbf{x}) = 0, \quad \mathbf{x} \in \Omega, \tag{1}$$

where Δ is the Laplace operator and $\kappa(\kappa \neq 0)$ is a complex number known as the wave number. In the case when κ is purely imaginary, i.e. $\kappa = \mathrm{i}\lambda$ with $\mathrm{i} = \sqrt{-1}$ and $\lambda \in \mathbb{R}$, Eq. (1) is also known as the modified Helmholtz equation and models heat conduction in fins [1]. On eliminating the imaginary unit, Eq. (1) with κ purely imaginary may be recast as

$$(\Delta - \lambda^2)u(\mathbf{x}) = 0, \quad \mathbf{x} \in \Omega. \tag{2}$$

In this paper, we consider only the cases when κ is real and purely imaginary, and for the ease of the presentation, Eqs. (1) and (2) are henceforth referred to as the Helmholtz and modified Helmholtz equations, respectively.

Let $\mathbf{n}(\mathbf{x})$ be the unit outward normal vector at the boundary point $\mathbf{x} \in \Gamma$ and $\phi(\mathbf{x})$ the normal derivative of the primary field $u(\mathbf{x})$ at $\mathbf{x} \in \Gamma$, also termed as the normal flux in the case of the modified Helmholtz equation, namely

$$\phi(\mathbf{x}) := \frac{\partial u(\mathbf{x})}{\partial \mathbf{n}} = \nabla u(\mathbf{x}) \cdot \mathbf{n}(\mathbf{x}), \quad \mathbf{x} \in \Gamma. \tag{3}$$

Assume that the governing partial differential equation (1) or (2) is subjected to the following Cauchy boundary conditions

$$\mathscr{B}_1 u(\mathbf{x}) = g(\mathbf{x}), \quad \mathscr{B}_2 u(\mathbf{x}) = h(\mathbf{x}), \quad \mathbf{x} \in \Gamma_1, \tag{4}$$

where $\Gamma_1 \subset \Gamma$ is the accessible part of the boundary and $\mathscr{B}_j$, $j = 1, 2$, are two linear operators prescribing the boundary conditions, i.e. $j = 1$ and $j = 2$ for Dirichlet and Neumann boundary conditions, respectively. The inverse problem consists of reconstructing the boundary conditions on the remaining part of the boundary $\Gamma_2 = \Gamma \backslash \Gamma_1$.

This problem, termed as the Cauchy problem, is much more difficult to solve than the forward problem both mathematically and numerically due to its severe ill-posed nature. Holmgren's theorem on the unique continuation of solutions to elliptic partial differential equations ensures the uniqueness of the solution to the Cauchy problem, see e.g. Colton and Kress [4]. However, the solution may not exist. Moreover, even if the solution exists, this is not continuously dependent on the data. This instability property has significant practical importance as the boundary data are based on experimental measurements and hence they cannot be determined accurately.

Furthermore, in addition to the Cauchy problem given by Eqs. (1) or (2) and (4), we also investigate the following inverse boundary value problem associated with the governing partial differential equation (1) or (2)

$$\mathscr{B}_j u(\mathbf{x}) = g(\mathbf{x}), \ \ \mathbf{x} \in \Gamma_1, \quad \mathscr{I} u(\mathbf{x}) = \tilde{u}(\mathbf{x}), \ \ \mathbf{x} \in \Omega_{\mathrm{int}} \subset \Omega, \tag{5}$$

where $j \in \{1, 2\}$ depends upon the type of boundary conditions available, $\mathscr{I}$ is the identity operator and $\Omega_{\mathrm{int}} \subset \Omega$. The uniqueness of the solution is guaranteed by the unique continuation principle and this problem corresponds to the case when the data are internal measurements.

Please cite this article as: Jin B, Marin L. The plane wave method for inverse problems associated with Helmholtz-type equations. Eng Anal Bound Elem (2007), doi:10.1016/j.enganabound.2007.08.005

3. Numerical scheme

In this section, we describe the numerical scheme for the inverse problem, namely the PWM in conjunction with the TSVD. The connection of the PWM to the MFS and BKM is also briefly discussed.

3.1. The plane wave method

In both iterative and direct methods, the partial differential equation must be discretized. Meshfree methods have received much attention from both scientific and engineering community in recent years, see e.g. Griebel and Schweitzer [29] and Liu [30], due to the absence of the mesh in comparison with their more traditional counterparts, such as the finite element method and BEM. Boundary-type meshfree methods, such as the MFS [31,32] and BKM [33,34], are popular for solving numerically homogeneous problems and have been successfully applied to inverse problems, see Jin and Zheng [20,21], Marin and Lesnic [22], Marin [23] and Wei et al. [24]. The PWM is a ridge function collocation technique for discretizing homogeneous problems, see e.g. Pinkus [35], and hence it is also truly boundary-type and inherently meshfree.

The PWM approximates the solution of a homogeneous partial differential equation by a linear combination of plane waves. The plane wave for the Helmholtz and modified Helmholtz equations in $\mathbb{R}^d$ is given by

$$u^*(\mathbf{x},\mathbf{d}) = \mathrm{e}^{\mathrm{i}\kappa\mathbf{x}\cdot\mathbf{d}}, \quad \mathbf{x}\in\mathbb{R}^d \tag{6}$$

and

$$u^*(\mathbf{x},\mathbf{d}) = \mathrm{e}^{\lambda\mathbf{x}\cdot\mathbf{d}}, \quad \mathbf{x}\in\mathbb{R}^d, \tag{7}$$

respectively, where $\mathbf{d}\in\mathbb{S}^{d-1}$ is a unit vector in $\mathbb{R}^d$ and $\mathbf{x}\cdot\mathbf{d}$ denotes the inner product of two vectors $\mathbf{x}=(x_1,x_2,\ldots,x_d)^{\mathrm{T}}$ and $\mathbf{d}=(d_1,d_2,\ldots,d_d)^{\mathrm{T}}$, namely

$$\mathbf{x}\cdot\mathbf{d} = \sum_{k=1}^{d} x_k d_k. \tag{8}$$

In the PWM, one seeks an approximate solution, $u(\mathbf{x})$, in the form

$$u(\mathbf{x}) = \sum_{j=1}^{n_s} a_j G_j(\mathbf{x}), \quad \mathbf{x}\in\overline{\Omega}=\Omega\cup\Gamma, \tag{9}$$

where $G_j(\mathbf{x})=u^*(\mathbf{x},\mathbf{d}_j)$, $\{\mathbf{d}_j\}$ is the set of directions, n_s is the number of directions and $\{a_j\}$ are unknown coefficients to be determined.

Due to this special choice of the basis functions, the approximate solution $u(\mathbf{x})$ automatically satisfies the governing homogeneous partial differential equation. However, it does not necessarily satisfy the boundary conditions. The latter can be enforced by means of either the collocation method or the Galerkin method and, for simplicity, we employ the collocation method in the present study. Let $\{\mathbf{x}_i\}$ be a set of points on the boundary Γ_1. By collocating Eq. (4) at $\{\mathbf{x}_i\}$, we arrive at the following system of linear algebraic equations

$$g(\mathbf{x}_i) = \sum_{j=1}^{n_s} a_j \mathscr{B}_1 G_j(\mathbf{x}_i), \quad i=1,2,\ldots,n_1, \tag{10}$$

$$h(\mathbf{x}_i) = \sum_{j=1}^{n_s} a_j \mathscr{B}_2 G_j(\mathbf{x}_i), \quad i=n_1+1,\ldots,n_1+n_2, \tag{11}$$

where n_1 and n_2 are the numbers of collocation points on the boundary Γ_1 for the boundary conditions defined by $\mathscr{B}_1$ and $\mathscr{B}_2$, respectively.

Briefly, we obtain the following system of linear algebraic equations:

$$\mathbf{A}\mathbf{a} = \mathbf{b}, \tag{12}$$

where $\mathbf{A}=(A_{ij})\in\mathbb{C}^{n\times n_s}$ is the interpolation matrix, $\mathbf{a}=(a_1,a_2,\ldots,a_{n_s})^{\mathrm{T}}\in\mathbb{C}^{n_s}$ is the vector containing the unknown coefficients, $\mathbf{b}=(g(\mathbf{x}_1),\ldots,g(\mathbf{x}_{n_1}),h(\mathbf{x}_{n_1+1}),\ldots,h(\mathbf{x}_n))^{\mathrm{T}}\in\mathbb{C}^n$ is the vector containing the given boundary data and $n=n_1+n_2$. More precisely, the entries A_{ij} of the interpolation matrix $\mathbf{A}$ are defined by

$$A_{ij} = \begin{cases} \mathscr{B}_1 G_j(\mathbf{x}_i), & i=1,2,\ldots,n_1,\ j=1,2,\ldots,n_s,\\ \mathscr{B}_2 G_j(\mathbf{x}_i), & i=n_1+1,\ldots,n,\ j=1,2,\ldots,n_s. \end{cases} \tag{13}$$

The system of linear algebraic equations (12) is often severely ill-conditioned. Its accurate and stable solution is crucial for obtaining physically meaningful numerical results and this will be discussed in detail in the next subsection.

The use of plane waves for solving partial differential equations dates at least back to early 1950s, see e.g. John [36]. Numerically, it has been successfully applied to eigenvalue problems (quantum billiards) by Heller [37] and Li et al. [38] and wave guide calculations by Sakoda [39]. Alves and Valtchev [40,41] applied the PWM to the numerical solution of the Helmholtz equation and, more recently, Li [42] studied the performance of this method for the modified Helmholtz equation. The PWM is closely related to the MFS. The fundamental solutions of the Helmholtz and modified Helmholtz equations with the source point located at $\mathbf{y}$ are given by

$$u^{\#}(\mathbf{x},\mathbf{y}) = \begin{cases} \dfrac{\mathrm{i}}{4}H_0^{(1)}(\kappa r), & \mathbf{x}\in\mathbb{R}^2,\\ \dfrac{1}{4\pi r}\mathrm{e}^{\mathrm{i}\kappa r}, & \mathbf{x}\in\mathbb{R}^3 \end{cases} \tag{14}$$

and

$$u^{\#}(\mathbf{x},\mathbf{y}) = \begin{cases} \dfrac{1}{2\pi}K_0(\lambda r), & \mathbf{x}\in\mathbb{R}^2,\\ \dfrac{1}{4\pi r}\mathrm{e}^{-\lambda r}, & \mathbf{x}\in\mathbb{R}^3 \end{cases} \tag{15}$$

respectively, where $r=\|\mathbf{x}-\mathbf{y}\|_2$ and $\|\cdot\|_2$ denotes the Euclidean norm. Here $H_0^{(1)}$ is the Hankel function of the first kind of order zero and K_0 is the modified Bessel function of the second kind of order zero. Note that the following asymptotic expansions, see e.g. Abramowitz and

Please cite this article as: Jin B, Marin L. The plane wave method for inverse problems associated with Helmholtz-type equations. Eng Anal Bound Elem (2007), doi:10.1016/j.enganabound.2007.08.005

Stegun [43]

$$u^{\#}(\mathbf{x},\mathbf{y}) = \begin{cases} \frac{e^{i\kappa r'}e^{i\pi/4}}{\sqrt{8\pi\kappa r'}}[e^{-i\kappa\mathbf{x}\cdot\widehat{\mathbf{y}}} + \mathcal{O}(r'^{-1})], & \mathbf{x}\in\mathbb{R}^2, \\ \frac{e^{i\kappa r'}}{4\pi r'}[e^{-i\kappa\mathbf{x}\cdot\widehat{\mathbf{y}}} + \mathcal{O}(r'^{-1})], & \mathbf{x}\in\mathbb{R}^3 \end{cases} \quad \text{as } r'\to\infty \tag{16}$$

and

$$u^{\#}(\mathbf{x},\mathbf{y}) = \begin{cases} \frac{e^{-\lambda r'}}{\sqrt{8\pi\lambda r'}}[e^{\lambda\mathbf{x}\cdot\widehat{\mathbf{y}}} + \mathcal{O}(r'^{-1})], & \mathbf{x}\in\mathbb{R}^2, \\ \frac{e^{-\lambda r'}}{4\pi r'}[e^{\lambda\mathbf{x}\cdot\widehat{\mathbf{y}}} + \mathcal{O}(r'^{-1})], & \mathbf{x}\in\mathbb{R}^3 \end{cases} \quad \text{as } r'\to\infty \tag{17}$$

relation can be obtained for the Helmholtz equation, whose nonsingular general solution with the source point located at $\mathbf{y}$ is given by

$$u^{\#}(\mathbf{x},\mathbf{y}) = \begin{cases} \frac{1}{2\pi}J_0(\kappa r), & \mathbf{x}\in\mathbb{R}^2, \\ \frac{1}{4\pi r}\sin(\kappa r), & \mathbf{x}\in\mathbb{R}^3. \end{cases} \tag{20}$$

On taking the imaginary part of Eq. (16), we obtain, see Abramowitz and Stegun [43]

The plane wave could be regarded as a ridge function, see

$$u^{\#}(\mathbf{x},\mathbf{y}) = \begin{cases} \frac{1}{\sqrt{2\pi^3\kappa r'}}\left[\cos\left(\kappa r' - \frac{\pi}{4} - \kappa\mathbf{x}\cdot\widehat{\mathbf{y}}\right) + \mathcal{O}(r'^{-1})\right], & \mathbf{x}\in\mathbb{R}^2, \\ \frac{1}{4\pi r'}[\sin(\kappa r' - \kappa\mathbf{x}\cdot\widehat{\mathbf{y}}) + \mathcal{O}(r'^{-1})], & \mathbf{x}\in\mathbb{R}^3 \end{cases} \quad \text{as } r'\to\infty. \tag{21}$$

are valid for the Helmholtz and modified Helmholtz equations, respectively. Here $r' = \|\mathbf{y}\|_2$ and $\widehat{\mathbf{y}} = \mathbf{y}/r'$ is a unit vector in the direction of $\mathbf{y}$. Therefore, the PWM could be regarded as the MFS with the source points located at infinity. Recall that the accuracy of the MFS usually increases as the fictitious boundary moves away from the physical one and theoretically the optimal one should be placed at infinity [32]. However, numerical experiments show that the accuracy deteriorates significantly due to rounding errors when the distance between the fictitious and physical boundaries is very large. Consequently, the PWM also features the fast convergence of the MFS for smooth solutions and works practically identical with the MFS with source points placed far away from the physical boundary [41]. However, the PWM surpasses the MFS, in the sense that it avoids the controversial requirement of constructing a fictitious boundary outside of the physical domain since the plane waves are nonsingular.

The PWM is also closely related to the BKM [34]. The nonsingular general solution of the modified Helmholtz equation with the source point located at $\mathbf{y}$ is given by

$$u^{\#}(\mathbf{x},\mathbf{y}) = \begin{cases} \frac{1}{2\pi}I_0(\lambda r), & \mathbf{x}\in\mathbb{R}^2, \\ \frac{1}{4\pi r}\sinh(\lambda r), & \mathbf{x}\in\mathbb{R}^3, \end{cases} \tag{18}$$

where I_0 is the modified Bessel function of the first kind of order zero. Note that the following asymptotic expansion holds, see e.g. Abramowitz and Stegun [43]

$$u^{\#}(\mathbf{x},\mathbf{y}) = \begin{cases} \frac{e^{\lambda r'}}{\sqrt{8\pi^3\lambda r'}}[e^{-\lambda\mathbf{x}\cdot\widehat{\mathbf{y}}} + \mathcal{O}(r'^{-1})], & \mathbf{x}\in\mathbb{R}^2, \\ \frac{e^{\lambda r'}}{8\pi r'}[e^{-\lambda\mathbf{x}\cdot\widehat{\mathbf{y}}} + \mathcal{O}(r'^{-1})] - \frac{e^{-\lambda r'}}{8\pi r'}[e^{\lambda\mathbf{x}\cdot\widehat{\mathbf{y}}} + \mathcal{O}(r'^{-1})], & \mathbf{x}\in\mathbb{R}^3 \end{cases}$$
as $r'\to\infty$. (19)

Therefore, the PWM could be regarded as the BKM with source points placed at infinity. Numerical experiments indicate that in the BKM with source points moving away from the physical boundary, the conditioning of the interpolation matrix improves considerably. A similar Pinkus [35], and, therefore, existing theoretical results for ridge functions may be adapted for the PWM. The density and fundamentality of the plane waves and general ridge functions have been established by Alves and Valtchev [40,41] and Li [42], and Kroó [44], respectively. Moreover, it was also shown that an appropriately chosen superposition of ridge functions could converge at a good rate to the underlying function, see e.g. Barron [45] and Petrushev [46].

3.2. Regularization techniques

The use of collocation methods, in conjunction with global basis functions, often results in an ill-conditioned coefficient matrix. In addition, the ill-posedness of the inverse problem also carries over to the discretized problem, i.e. Eq. (12). Consequently, the interpolation matrix $\mathbf{A}$ is often severely ill-conditioned and an accurate and stable numerical solution to the associated system of linear algebraic equations is required. Regularization methods are among the most popular and successful techniques for solving stably and accurately ill-conditioned matrix equations, see Hansen [47]. In our computations, we use the TSVD to solve the matrix equation arising from the PWM discretization.

The SVD of a matrix $\mathbf{A}\in\mathbb{C}^{n\times n_s}(n\geqslant n_s)$ is given by

$$\mathbf{A} = \mathbf{U}\mathbf{\Sigma}\mathbf{V}^{\mathrm{H}}, \tag{22}$$

where $\mathbf{U} = [\mathbf{u}_1,\mathbf{u}_2,\ldots,\mathbf{u}_n]$ and $\mathbf{V} = [\mathbf{v}_1,\mathbf{v}_2,\ldots,\mathbf{v}_{n_s}]$ are unitary matrices with column vectors called the left and the right singular vectors, respectively, whilst $\mathbf{\Sigma} = \mathrm{diag}(\sigma_1,\sigma_2,\ldots,\sigma_{n_s})$ is a diagonal matrix with nonnegative diagonal elements in non-increasing order which are the singular values of $\mathbf{A}$. Here the superscript H denotes the conjugate transpose of a complex matrix.

A convenient measure for the conditioning of Eq. (12) is the condition number of the matrix $\mathbf{A}$ defined as the ratio

Please cite this article as: Jin B, Marin L. The plane wave method for inverse problems associated with Helmholtz-type equations. Eng Anal Bound Elem (2007), doi:10.1016/j.enganabound.2007.08.005

of the largest singular value to the smallest one, i.e.

$$\mathrm{Cond}(\mathbf{A}) = \frac{\sigma_1}{\sigma_{n_s}}. \tag{23}$$

On using the SVD, the solution $\mathbf{a}$ to Eq. (12) can be succinctly written as a linear combination of the right singular vectors, namely

$$\mathbf{a} = \sum_{i=1}^{k} \frac{\mathbf{u}_i^{\mathrm{H}}\mathbf{b}}{\sigma_i}\mathbf{v}_i, \tag{24}$$

where k is the rank of the matrix $\mathbf{A}$. Ill-conditioned matrices often have many small singular values clustering around zero and, therefore, the solution to Eq. (12) by standard methods may be dominated by the contribution of the small singular values. One simple remedy is to truncate the above summation by considering an approximate solution, $\mathbf{a}^p$, given by

$$\mathbf{a}^p = \sum_{i=1}^{p} \frac{\mathbf{u}_i^{\mathrm{H}}\mathbf{b}}{\sigma_i}\mathbf{v}_i, \tag{25}$$

where $p \leqslant k$ is the regularization parameter which determines when one starts to leave out small singular values. This method is known as the TSVD in the inverse problem community, see e.g. Hansen [47].

The regularization parameter p plays a crucial role in the performance of the TSVD. Several algorithms have been suggested for its appropriate choice, such as the discrepancy principle, generalized cross-validation and L-curve criterion, see Hansen [47]. Numerically, the L-curve criterion is robust and stable with respect to both uncorrelated and highly correlated noise and works effectively with certain classes of practical problems, see Hansen [47] and Hansen and O'Leary [48]. In the present study, we employ the L-curve criterion in order to determine the optimal regularization parameter.

The L-curve for the TSVD is defined by

$$L = \{(\log\|\mathbf{A}\,\mathbf{a}^i - \mathbf{b}\|_2, \log\|\mathbf{a}^i\|_2) | i = 1, 2, \ldots, k\}. \tag{26}$$

According to the L-curve criterion, the optimal regularization parameter is located at the corner of the curve defined by Eq. (26) since a good tradeoff between the residual and solution norms is achieved at this point. Several algorithms for locating the corner have been proposed, such as the maximum-curvature method, the conic fitting method and the triangle method. In the present study, we mainly employ the maximum-curvature method, see Hansen [47]. However, the curvature of the parametric spline is sensitive to the knot distribution and occasionally the located corner is not suitable, see Hansen and O'Leary [48]. Therefore, visual inspection is also used as an auxiliary procedure.

4. Numerical results and discussion

In this section, we present the numerical results obtained using the proposed scheme, namely the PWM, in conjunction with the TSVD, for several two- and three-dimensional benchmark examples in both smooth and piecewise smooth geometries. The convergence and stability of the proposed method with respect to increasing the number of collocation points and the number of directions, and decreasing the amount of noise added into the data, respectively, are analysed. In addition, a comparison with other meshless methods is also performed.

4.1. Examples

The domains under consideration and the accessible, Γ_1, and inaccessible, $\Gamma_2 = \Gamma \backslash \Gamma_1$, parts of the boundary Γ of the solution domains are given by:

Domain 1: (Unit disk: Two-dimensional smooth domain)

$$\begin{aligned}
&\Omega = \{(x_1, x_2) | x_1^2 + x_2^2 < 1\},\\
&\Gamma_1 = \{(r, \theta) | r = 1, 0 \leqslant \theta < \pi\},\\
&\Gamma_2 = \{(r, \theta) | r = 1, \pi \leqslant \theta < 2\pi\},
\end{aligned} \tag{27}$$

where (r, θ) are the polar coordinates corresponding to the point $\mathbf{x} = (x_1, x_2)$.

Domain 2: (Complex domain: Two-dimensional piecewise smooth domain) The configuration of the complex domain $\widehat{\Omega}$ is schematically shown in Fig. 1(a), where the boundaries Γ_1 and Γ_2 are also indicated. Note that the geometry of the domain $\widehat{\Omega}$ involves re-entrant corners and sharp notches which have been deliberately designed to verify the efficiency of the proposed scheme for problems with an arbitrary geometry.

Domain 3: (Unit cube: Three-dimensional piecewise smooth domain)

$$\begin{aligned}
\widetilde{\Omega} &= \{(x_1, x_2, x_3) | -0.5 < x_1, x_2, x_3 < 0.5\},\\
\Gamma_1 &= \{(x_1, x_2, -0.5) | -0.5 < x_1, x_2 < 0.5\}\\
&\quad \cup \{(x_1, -0.5, x_3) | -0.5 < x_1, x_3 < 0.5\}\\
&\quad \cup \{(-0.5, x_2, x_3) | -0.5 < x_2, x_3 < 0.5\},\\
\Gamma_2 &= \{(x_1, x_2, 0.5) | -0.5 < x_1, x_2 < 0.5\}\\
&\quad \cup \{(x_1, 0.5, x_3) | -0.5 < x_1, x_3 < 0.5\}\\
&\quad \cup \{(0.5, x_2, x_3) | -0.5 < x_2, x_3 < 0.5\}.
\end{aligned} \tag{28}$$

For the convenience of comparison and illustration of the accuracy, convergence and stability of the proposed scheme, we consider the test examples listed in Table 1, where Y_0 is the Bessel function of the second kind of order zero. Several examples are taken from Jin and Zheng [20,21] and Marin [23]. Example 1 is adopted to demonstrate the regularizing effect of the TSVD and investigate the convergence of the PWM. Examples 2 and 3 are considered for comparing the proposed numerical scheme with other meshfree methods, whilst Examples 4–7 are used to demonstrate the stability and efficiency of the present method for smooth and piecewise smooth, two- and three-dimensional geometries.

The boundary conditions on the boundary Γ_1 defined by the operators $\mathscr{B}_1$ and $\mathscr{B}_2$ are taken to be the Dirichlet and Neumann boundary conditions, respectively. Unless otherwise specified, the number of collocation points on the

Please cite this article as: Jin B, Marin L. The plane wave method for inverse problems associated with Helmholtz-type equations. Eng Anal Bound Elem (2007), doi:10.1016/j.enganabound.2007.08.005

boundary Γ_1 is taken to be 15 for the circular domain Ω, 24 for the complex domain $\widehat{\Omega}$ and 147 for the cube domain $\widetilde{\Omega}$, with the mention that the same collocation points are used for both types of boundary conditions. The distribution of the collocation points on the boundary Γ_1 in the case of the complex domain $\widehat{\Omega}$ is schematically shown in Fig. 1(a), whilst the distribution of the boundary collocation points on Γ_1 and scattered internal measurements for the domain Ω is presented in Fig. 1(b). The number of directions is taken to be the same as the number of boundary collocation points, i.e. $n_s = n$, such that the resulting interpolation matrix is square. The uniformity of the direction distribution could affect the accuracy of the numerical results significantly, see Alves and Valtchev [41]. In the two-dimensional case, the directions are uniformly distributed on the unit circle, whereas in the three-dimensional case, they are quasi-uniformly distributed on the unit sphere by employing an optimization procedure, see Ling [49].

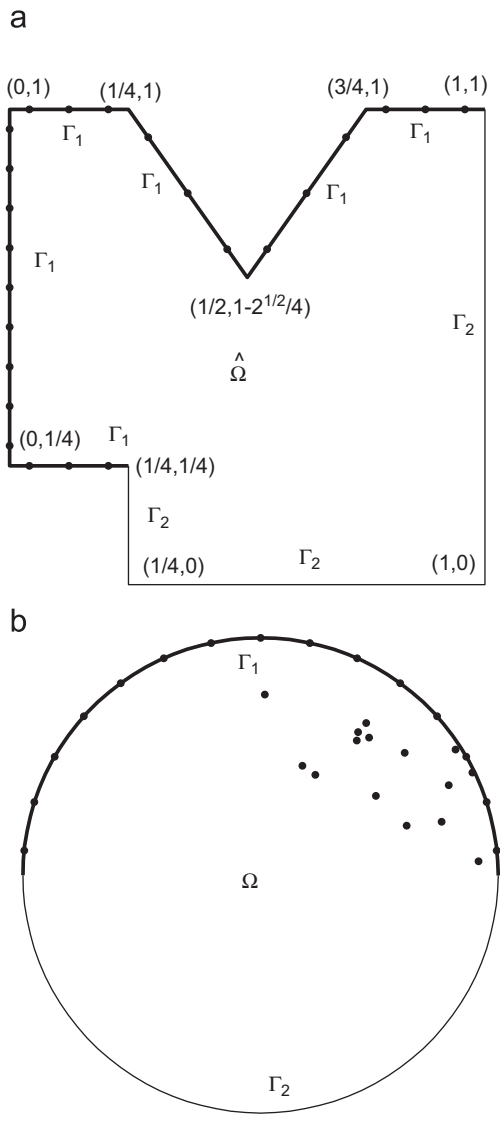

Fig. 1. (a) Schematic diagram of the domain $\widehat{\Omega}$ and the corresponding distribution of the boundary collocation points (•) on Γ_1. (b) The distribution of the boundary collocation points on Γ_1 and scattered internal measurements (•) for the domain Ω.

In real-world inverse problems, the known boundary data are measured and, therefore, contaminated by inherent measurement errors. For all examples investigated in this paper, the simulated noisy data are generated using the following formula:

$$\tilde{b}_i = b_i(1 + \varepsilon\zeta), \quad i = 1, 2, \ldots, n, \tag{29}$$

where ε indicates the level of noise added into the data and ζ is a normally distributed random variable with zero mean and unit standard deviation. In our computations, the random variable ζ is realized using the Matlab function `randn()`.

To measure the accuracy of a numerical approximation $\tilde{f}$ to the function f, we use relative error defined as

$$\mathrm{rel}(f) = \frac{\sqrt{\sum_{i=1}^{N}(f_i - \tilde{f}_i)^2}}{\sqrt{\sum_{i=1}^{N} f_i^2}}, \tag{30}$$

where f_i and $\tilde{f}_i$ are the exact and numerical solutions evaluated at the point $\mathbf{x}_i \in \Gamma_2$, respectively, and N is the total number of testing points on the boundary Γ_2. In the case of the examples considered herein, $N = 40$ and 1200 for the two- and three-dimensional problems investigated, respectively, and the evaluated points are distributed uniformly on the boundary Γ_2.

Table 1
Test cases for the inverse problems investigated

Example	$u(\mathbf{x})$	κ, λ	Domain	Equation
1	$\sin(x_1)\sin(x_2)$	$\kappa = \sqrt{2}$	Ω	Helmholtz
2	$\sin(\sqrt{2}x_1)\sinh(x_2) + \cos(x_2)$	$\kappa = 1$	Ω	Helmholtz
3	$\sin(8x_1) + \sin(8x_2)$	$\kappa = 8$	Ω	Helmholtz
4	$Y_0\left(\sqrt{(x_1-5)^2 + (x_2-10)^2}\right)$	$\kappa = 1$	Ω	Helmholtz
5	$\sin(\sqrt{2}x_1)\sinh(x_2) + \cos(x_2)$	$\kappa = 1$	$\widehat{\Omega}$	Helmholtz
6	$\exp\left(x_1 + \frac{1}{2}x_2 + \frac{\sqrt{11}}{2}x_3\right)$	$\lambda = 2$	$\widetilde{\Omega}$	Modified Helmholtz
7	$\exp(2x_1 - x_2)$	$\lambda = \sqrt{5}$	Ω	ModifiedHelmholtz

Please cite this article as: Jin B, Marin L. The plane wave method for inverse problems associated with Helmholtz-type equations. Eng Anal Bound Elem (2007), doi:10.1016/j.enganabound.2007.08.005

4.2. Ill-posedness and regularization of the problem

Before presenting the numerical results for the inverse problems analysed in this paper, it is interesting to investigate the source of ill-conditioning of the coefficient matrix **A**, i.e. the ill-posedness of the discretization and the inverse problem, respectively. To do so, we consider Example 1 with $\varepsilon = 1\%$ noise added into both the Dirichlet and Neumann data, i.e. the Cauchy data.

The most prominent feature of Eq. (12) is its severe ill-conditioning and its cause is attributed to both the discretization method and ill-posedness of the problem. Collocation methods based on global basis functions, such as the PWM, MFS and BKM, often result in ill-conditioned coefficient matrices, see e.g. Galperin and Zheng [50]. The Cauchy problem for Helmholtz-type equations is severely ill-posed, see John [8] and Hrycak and Isakov [9], and this feature also carries over to the discrete problem. Fig. 2(a) shows the condition number of the matrix **A** for the forward (Dirichlet problem) and Cauchy problems corresponding to the Helmholtz equation with the wave number $\kappa = \sqrt{2}$ and $n = n_s$. For both the forward and inverse problems the condition number Cond(**A**) increases exponentially up to $n_s = 40$ and then oscillates slightly around 10^{18} due to the inherent rounding errors. However, the condition number for the inverse problem is greater than that corresponding to the forward problem by $\mathcal{O}(10^3)$. The wave number κ has a significant effect on the ill-conditioning of the matrix **A**. Fig. 2(b) illustrates the condition number for the Helmholtz equation with the wave number $\kappa = 8$. The overall pattern is similar to that for $\kappa = \sqrt{2}$, but the difference in the condition number Cond(**A**) for the forward and inverse problems now increases to $\mathcal{O}(10^6)$. Therefore, the ill-posed nature of the problem contributes significantly to the ill-conditioning of the matrix **A**. For comparison purposes, the condition number of the interpolation matrix arising from the MFS and BKM discretizations of the forward and inverse problems are presented in Figs. 3(a) and (b), respectively. Their overall tendency is practically identical to that of the PWM. However, the BKM levels off for a number of collocation points lower than that corresponding to the MFS and PWM.

Fig. 4(a) presents the exact and numerical solutions for the temperature $u(\mathbf{x})$ on the boundary Γ_2, obtained using the Gaussian elimination method. It can be seen from this figure that the numerical solution is highly oscillatory, deviates from the exact one by two orders in magnitude and, therefore, represents a very inaccurate approximation to the exact solution. The same conclusion holds for numerical results obtained using the LU factorization or the QR decomposition. Although not presented here, it is reported that the numerical boundary flux obtained using the Gaussian elimination and the aforementioned meshless methods, in the case of the direct problem for Example 1 with $\varepsilon = 1\%$ noise added into the Dirichlet data, represents a good approximation for its corresponding analytical

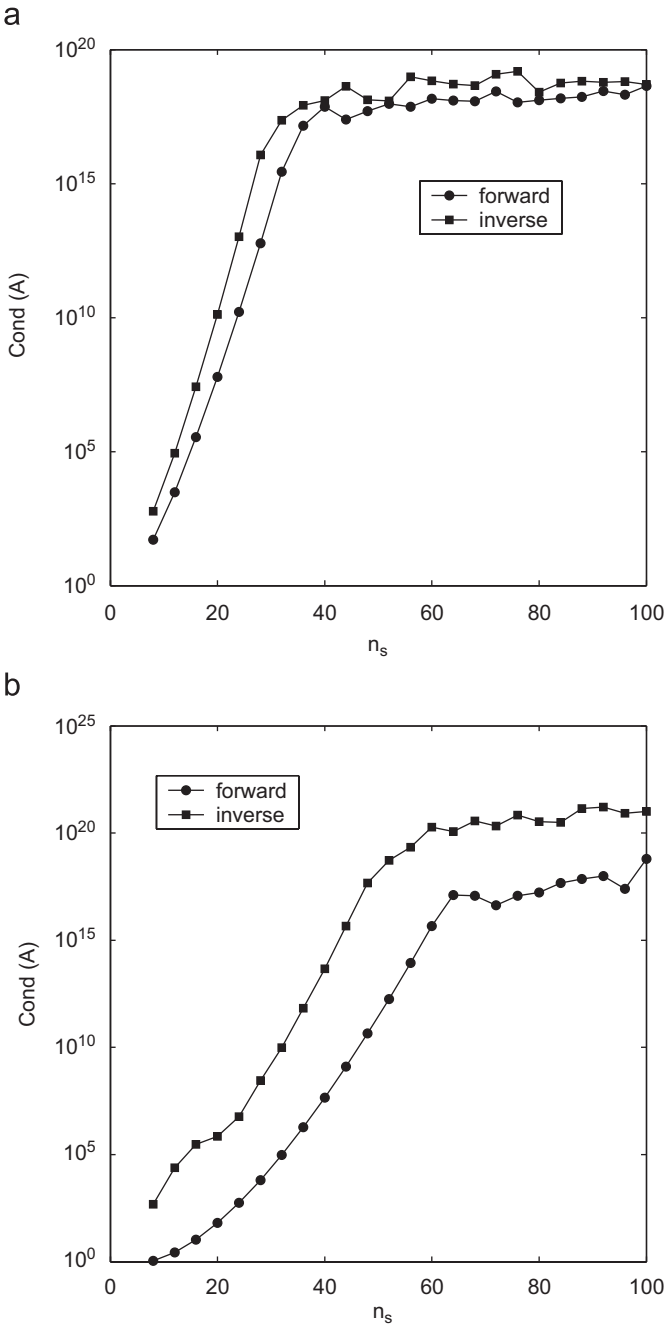

Fig. 2. The condition number, Cond(**A**), as a function of the number of directions, n_s, obtained using the PWM and the wave numbers (a) $\kappa = \sqrt{2}$ and (b) $\kappa = 8$.

value. However, these results can be improved by employing regularization methods. Therefore, we can conclude that it is mainly the severe ill-conditioning stemming from the inverse problem that precludes the use of standard methods for the resulting system of linear algebraic equations in the presence of noisy data.

To further expose the difficulty that occurs when solving the resulting PWM system of linear algebraic equations using standard methods, we present in Fig. 5(a) the singular value spectrum of the matrix **A**, the Fourier coefficients $|\mathbf{u}_i^{\mathrm{H}}\mathbf{b}|$ and the ratio $|\mathbf{u}_i^{\mathrm{H}}\mathbf{b}|/\sigma_i$, which is also

Please cite this article as: Jin B, Marin L. The plane wave method for inverse problems associated with Helmholtz-type equations. Eng Anal Bound Elem (2007), doi:10.1016/j.enganabound.2007.08.005

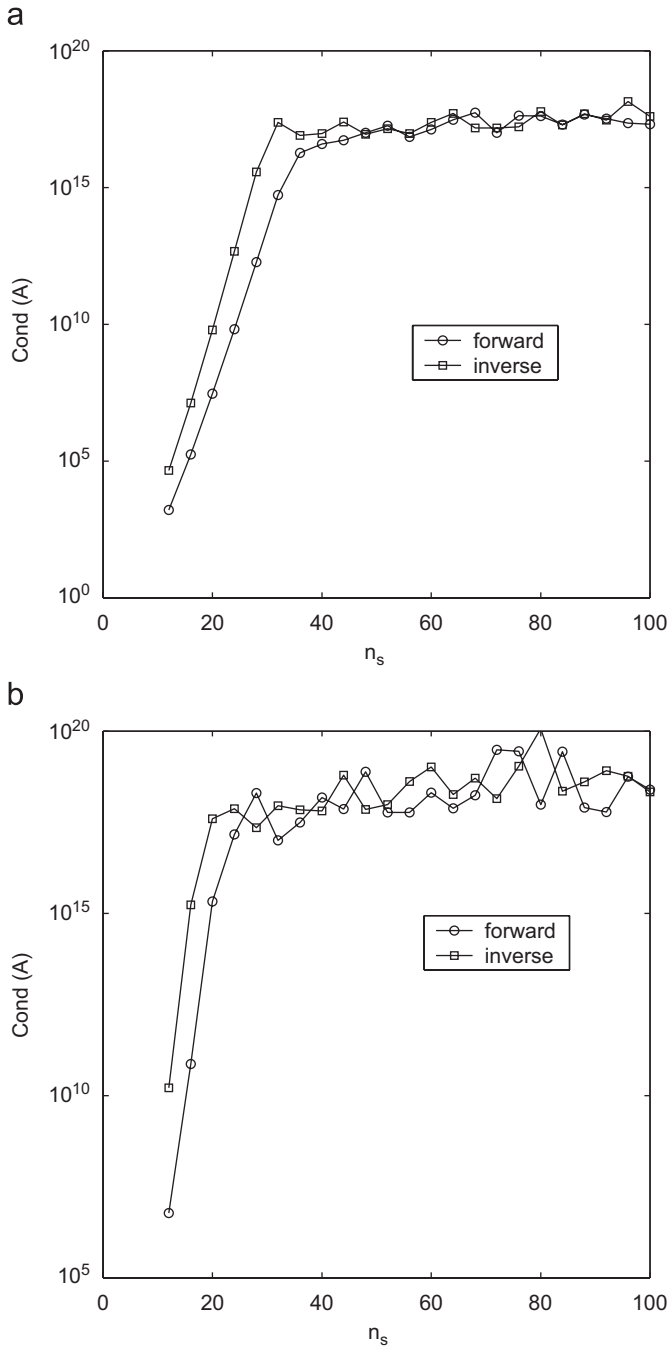

Fig. 3. The condition number, Cond(**A**), as a function of the number of source points, n_s, obtained using (a) the MFS, and (b) the BKM, and the wave number $\kappa = \sqrt{2}$.

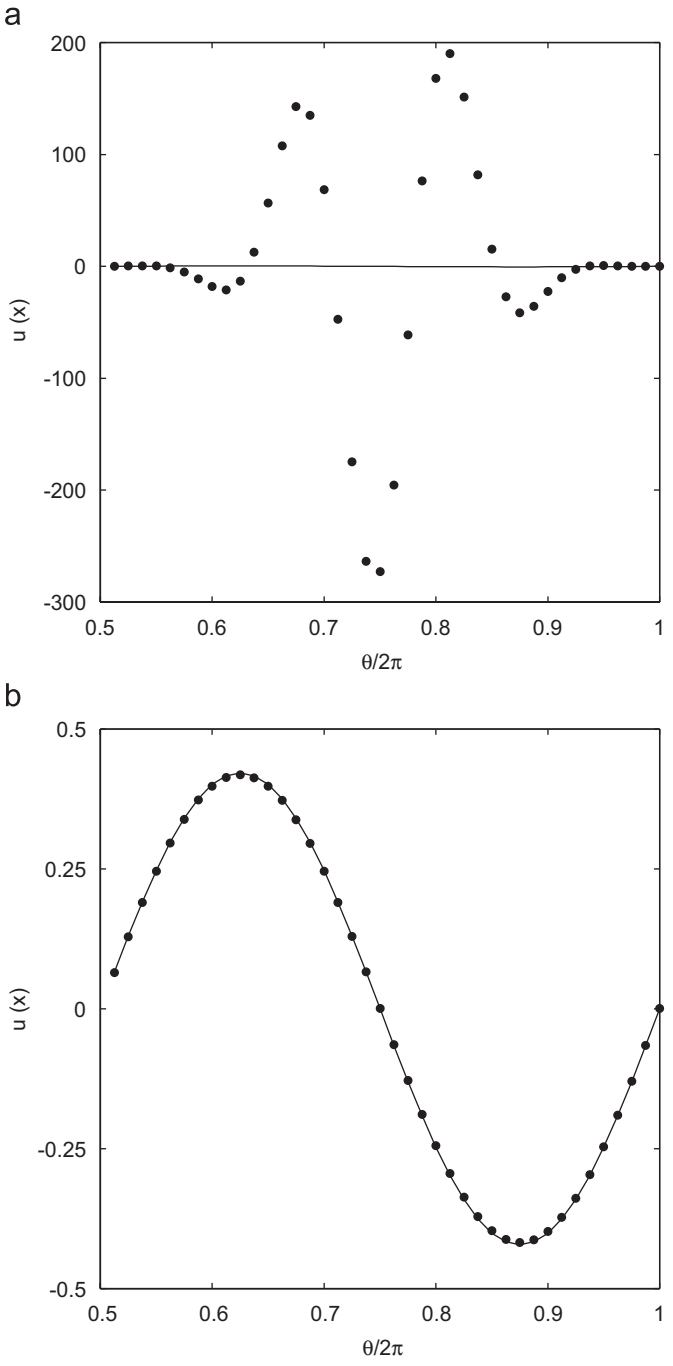

Fig. 4. The analytical (—) and numerical (•) temperatures, $u(\mathbf{x})$ on Γ_2, obtained using $\varepsilon = 1\%$ noise added into the Cauchy data, (a) the Gaussian elimination method, and (b) the TSVD, for Example 1.

known as the Picard plot in the literature, see e.g. Hansen [47]. The spectrum is abundant with small singular values and, moreover, the singular values decay gradually to zero without any obvious gap and eventually cluster around zero. However, the Fourier coefficients $|\mathbf{u}_i^{\mathrm{H}}\mathbf{b}|$ for $i \geqslant 10$ are approximately maintained at a level of $\mathcal{O}(10^{-2})$, which is statistically consistent with the fact that the noise level of the data is 1%, see Hansen [47]. Consequently, the ratio $|\mathbf{u}_i^{\mathrm{H}}\mathbf{b}|/\sigma_i$ blows up and may reach values of $\mathcal{O}(10^{13})$, which according to Eq. (24) render the solution obtained by standard methods completely dominated by the contributions from small singular values.

The TSVD alleviates the aforementioned difficulty by leaving out the contributions from small singular values and the TSVD-based results are shown in Fig. 4(b). It should be mentioned that the regularization parameter $p = 8$ is determined by the L-curve criterion and the corresponding L-curve is illustrated in Fig. 5(b). Note that the curve approximately consists of two distinct parts, namely the vertical (large p) and horizontal (small p) ones,

Please cite this article as: Jin B, Marin L. The plane wave method for inverse problems associated with Helmholtz-type equations. Eng Anal Bound Elem (2007), doi:10.1016/j.enganabound.2007.08.005

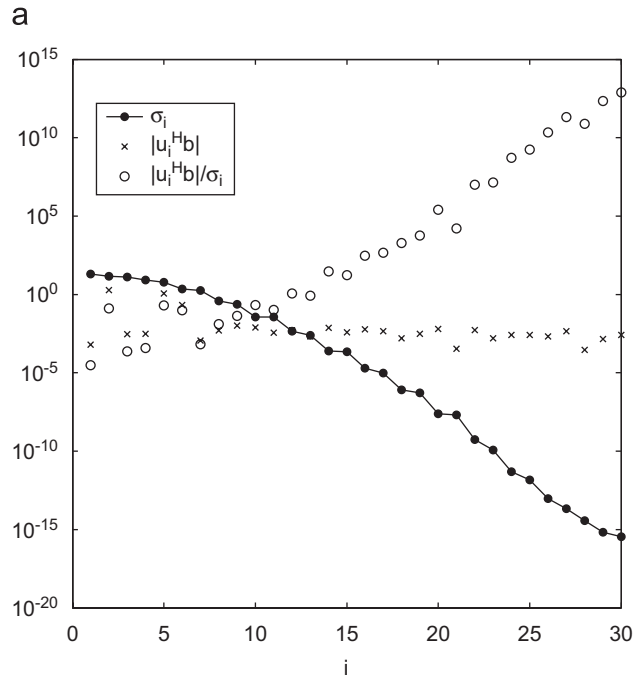

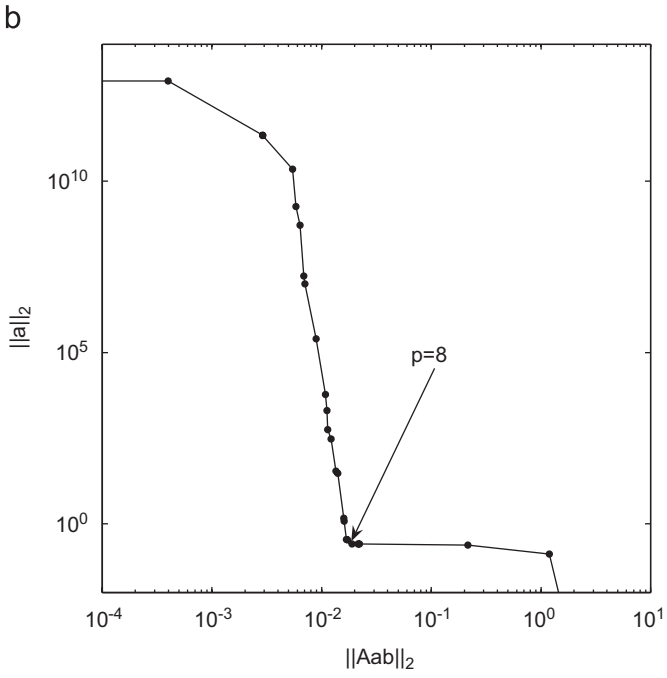

Fig. 5. (a) The Picard plot, and (b) the L-curve, obtained using $\varepsilon = 1\%$ noise added into the Cauchy data for Example 1.

with the mention that a good tradeoff between the solution and residual norms is achieved at the corner of the L-curve. The numerical solution retrieved by the TSVD is in excellent agreement with the exact one and the results indicate that the TSVD, in conjunction with the L-curve method, yields stable and accurate numerical results for noisy Cauchy data.

It should be mentioned that the present computations have been performed on a PC with 1.00 GB RAM using Matlab 6.5. The computational time as a function of the number of directions, n_s, obtained using the PWM, $n = n_s$, the wave number $\kappa = \sqrt{2}$ and $\varepsilon = 1\%$ noise added into the Cauchy data, for the inverse problem associated with Example 1 is shown in Fig. 6. The average computational time for 10 runs of the code was found to be 0.3 s, whilst less than 0.01 s were spent for the SVD calculations. The computational time allocated to the present numerical scheme is much less than that corresponding to the alternating iterative method or CGM, see e.g. Marin et al. [25,26], and thus the PWM + TSVD is computationally efficient. However, the time for computing the SVD is dominant when the size of the resulting system of linear algebraic equations reaches 1000, as can be seen from Fig. 6, since its flop count grows like $4n^2 n_s + 8nn_s^2 + 9n_s^3$, see Golub and Van Loan [51]. Therefore, the TSVD is not amenable with large-scale problems and more tractable alternatives should be employed. A possible approach in this case would be to adopt other computationally more efficient rank-revealing techniques, such as the UTV and URV decompositions, or iterative regularization methods, e.g. the GMRES and CGM.

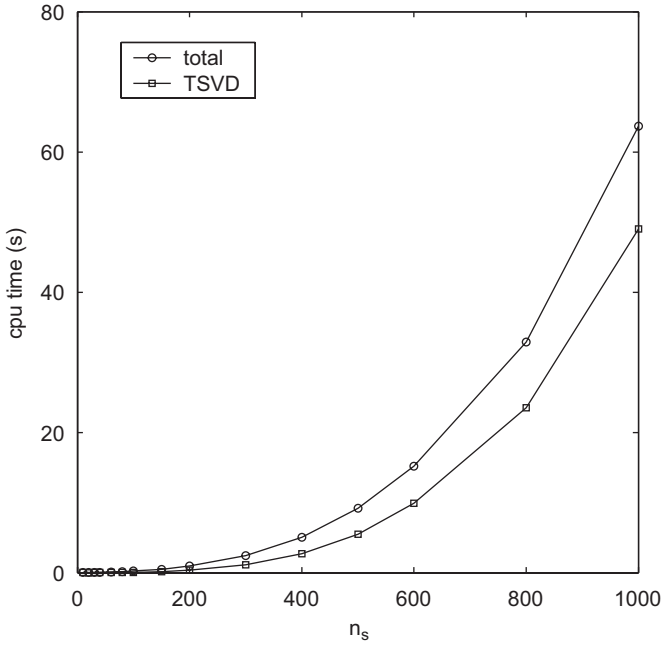

Fig. 6. The computational time as a function of the number of directions, n_s, obtained using the PWM, $n = n_s$, the wave number $\kappa = \sqrt{2}$ and $\varepsilon = 1\%$ noise added into the Cauchy data, for the inverse problem associated with Example 1.

4.3. Convergence analysis

In this section, we investigate the convergence of the scheme with respect to increasing the number of directions, n_s, and collocation points, n, for both exact and noisy data. In order to ensure the uniqueness of the solution to Eq. (12), we require that $n \geqslant n_s$.

Firstly, we consider the inverse problem under investigation with exact Cauchy data, with the mention that the corresponding system of linear algebraic equations is

Please cite this article as: Jin B, Marin L. The plane wave method for inverse problems associated with Helmholtz-type equations. Eng Anal Bound Elem (2007), doi:10.1016/j.enganabound.2007.08.005

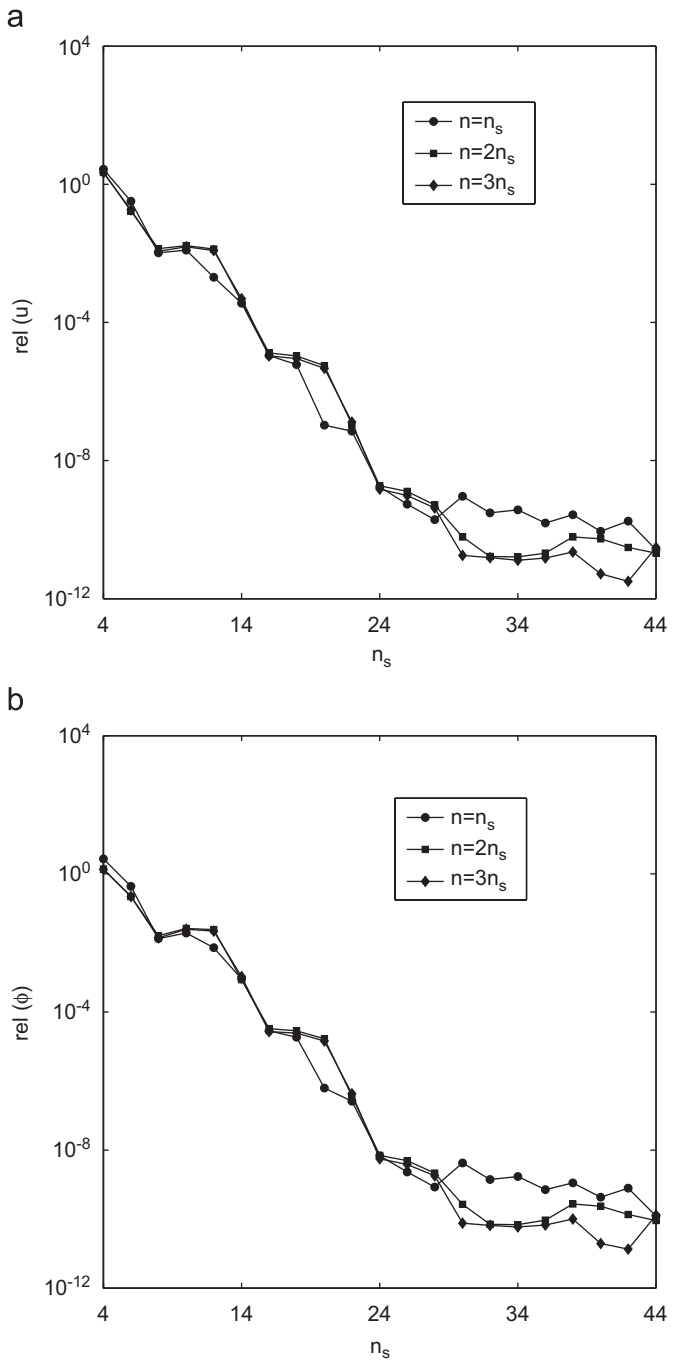

Fig. 7. The relative errors (a) rel(u), and (b) rel(ϕ), as functions of the number of directions, n_s, obtained using exact data and various values of the ratio n/n_s, for Example 1.

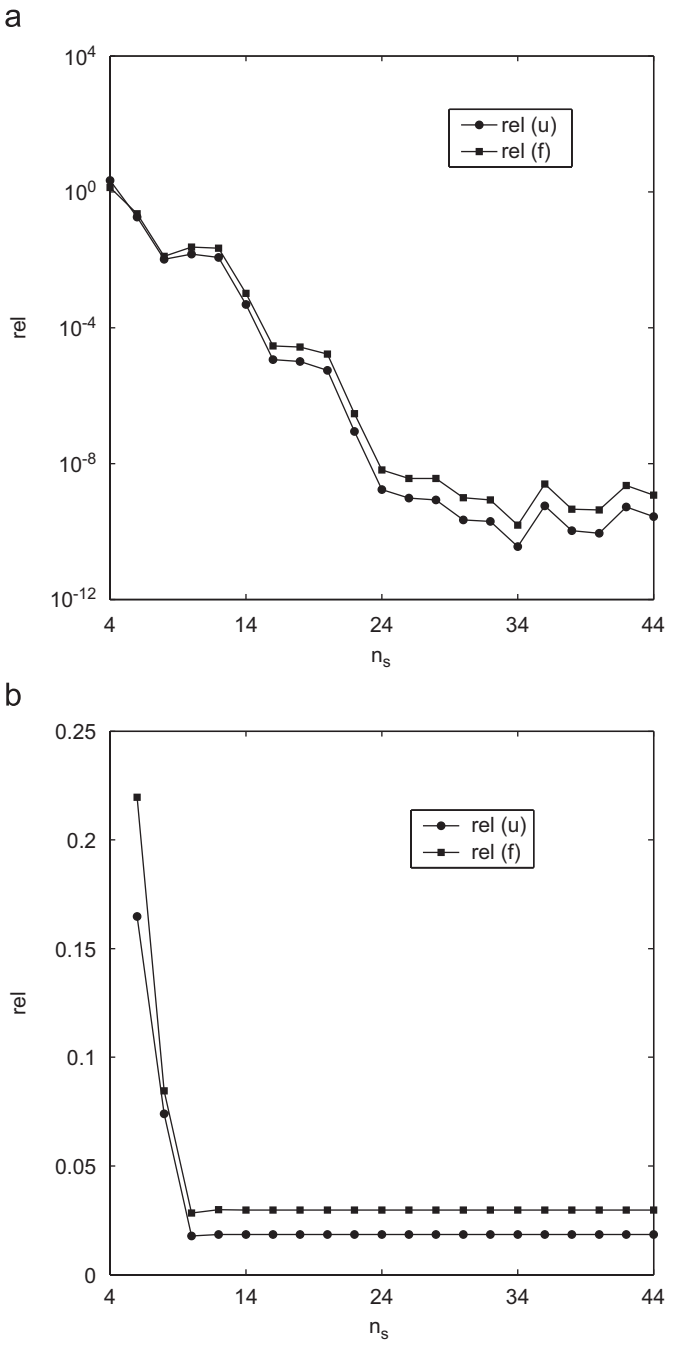

Fig. 8. The relative errors, rel(u) (•) and rel(ϕ) (■), as functions of the number of directions, n_s, obtained using $n = 40$ collocation points, (a) exact data, and (b) $\varepsilon = 3\%$ noise added into the Cauchy data, for Example 1.

solved by the Gaussian elimination method since no regularization is required in this case. The numerical results obtained for Example 1 by varying simultaneously both the number of collocation points, n, and directions, n_s, such that the ratio n/n_s is constant, are presented in Figs. 7(a) and (b) in terms of the relative errors rel(u) and rel(ϕ), respectively. Both these errors decrease exponentially as n_s attains a threshold value, after which they tend to level off. The convergence rate of rel(u) was found to be 13.8 and 13.0 for the ratios $n/n_s = 1, 2$ and $n/n_s = 3$, respectively, and hence the ratio n/n_s has a negligible effect on the convergence rate of the numerical solution. However, this ratio does improve slightly the accuracy for $n_s \geqslant 30$ at the expense of increased computational cost. Fig. 8(a) displays the results obtained by setting the number of collocation points to $n = 40$ and varying the number of directions, n_s. Again, both relative errors rel(u) and rel(ϕ) decrease exponentially up to $n_s = 30$ and then they slightly oscillate around 10^{-10}. The convergence rate of the errors rel(u) and rel(ϕ) was found to be 13.8 and

Please cite this article as: Jin B, Marin L. The plane wave method for inverse problems associated with Helmholtz-type equations. Eng Anal Bound Elem (2007), doi:10.1016/j.enganabound.2007.08.005

12.9, respectively, which is comparable with the case corresponding to the simultaneous increment of both n and n_s, such that n/n_s is constant. Note that for $n_s = 44$, we obtain an under-determined version of the PWM, for which the solution is not unique. However, the solution based on the TSVD is still well-defined [51] and the numerical results presented herein indicate that this under-determined version of the PWM also works well.

Further, we consider Example 1 with 3% noise added into the Cauchy data and the optimal truncation number, i.e. regularization parameter, p determined by the L-curve criterion. Fig. 8(b) illustrates the evolution of the relative errors rel(u) and rel(ϕ) with respect to the number of directions, n_s, and collocation points $n = 40$. It can be seen from this figure that both rel(u) and rel(ϕ) decrease as $4 \leqslant n_s \leqslant 10$, whilst a further increase in the number of directions does not result in a significant improvement of the numerical results. Fig. 9 presents the relative accuracies corresponding to the numerical results obtained in the case of Example 1 with 3% noise added into the Cauchy data, as functions of the number of directions, n_s, such that the ratio n/n_s is kept constant. The accuracy of the numerical results improves for $n_s \leqslant 12$ and a further increase in the number of directions, n_s, does not improve substantially the accuracy of the numerical results. It should also be mentioned that the ratio n/n_s does not influence significantly the relative errors rel(u) and rel(ϕ).

It should be mentioned that a low number of directions, namely $n_s = 12$, was found sufficient to obtain an accurate and stable numerical solution to the inverse problem associated with Example 1, for both exact and noisy data. Consequently, the size of the resulting matrix equation is quite small and this implies the computational efficiency of the proposed scheme. Although not presented herein, it is reported that similar results have been obtained for the other examples analysed in this paper.

4.4. Comparison with other meshless methods

The basic idea of the PWM is similar to that of the MFS and BKM, and a comparative study of the PWM and MFS for forward problems has been undertaken by Alves and Valtchev [41]. In this section, we compare the performance of the aforementioned meshless methods when employed for solving inverse problems associated with Helmholtz-type equations.

To do so, we consider Example 2 with exact boundary data. All the meshfree numerical methods considered are very accurate for solving inverse problems with exact boundary data. The absolute error distributions of the numerical results obtained by the PWM, MFS and BKM are shown in Fig. 10, where $n = n_s = 40$. The source points for the MFS are placed on a circle centred at the origin with radius 10, whilst those for the BKM are located on two arcs $\{(r,\theta) : r = 1, 0 \leqslant \theta \leqslant \pi\} \cup \{(r,\theta) : r = 0.8, 0 \leqslant \theta \leqslant \pi\}$, see e.g. Jin and Zheng [20]. The maximum absolute errors for the numerical boundary temperature $u(\mathbf{x})$ retrieved using the PWM, MFS and BKM were found to be 7.625×10^{-7}, 2.386×10^{-7} and 6.865×10^{-4}, respectively. The striking accuracy of the numerical results obtained by these methods is often attributed to their exponential convergence for smooth solutions, see e.g. Golberg and Chen [32], Hon and Chen [34] and Alves and Valtchev [41]. For the inverse problems under investigation, the numerical results obtained using the PWM are slightly less inaccurate than those retrieved by the MFS, with the mention that these meshless methods provide

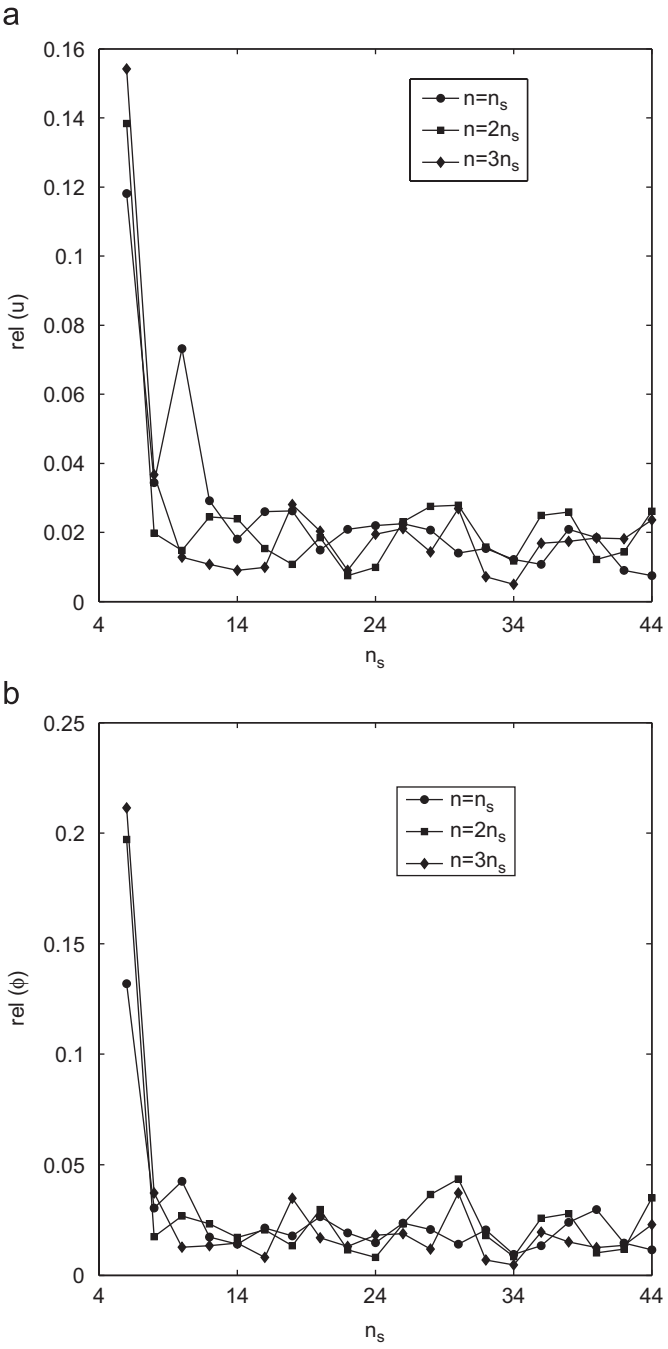

Fig. 9. The relative errors (a) rel(u), and (b) rel(ϕ), as functions of the number of directions, n_s, obtained using $\varepsilon = 3\%$ noise added into the Cauchy data and various values of the ratio n/n_s, for Example 1.

Please cite this article as: Jin B, Marin L. The plane wave method for inverse problems associated with Helmholtz-type equations. Eng Anal Bound Elem (2007), doi:10.1016/j.enganabound.2007.08.005

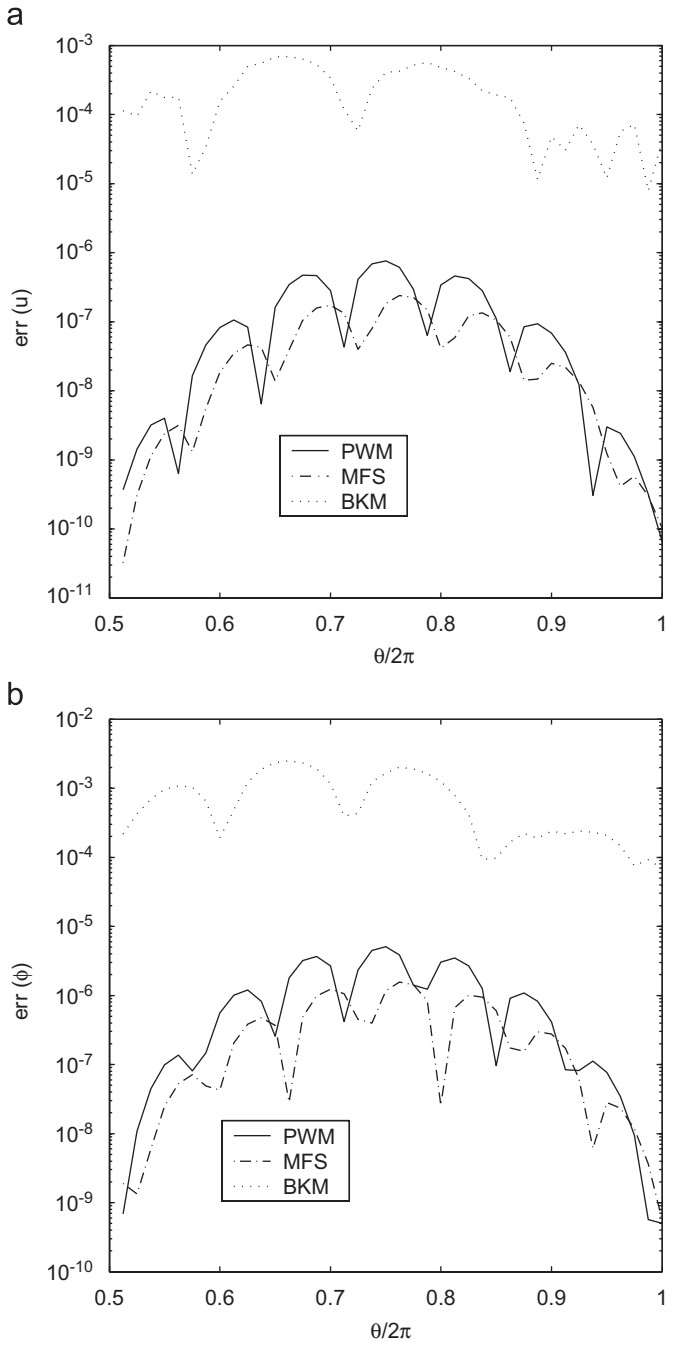

Fig. 10. The absolute errors (a) err(u), and (b) err(ϕ) on Γ_2, obtained using $n_s = 40$, $n = 40$ and exact data, for Example 2.

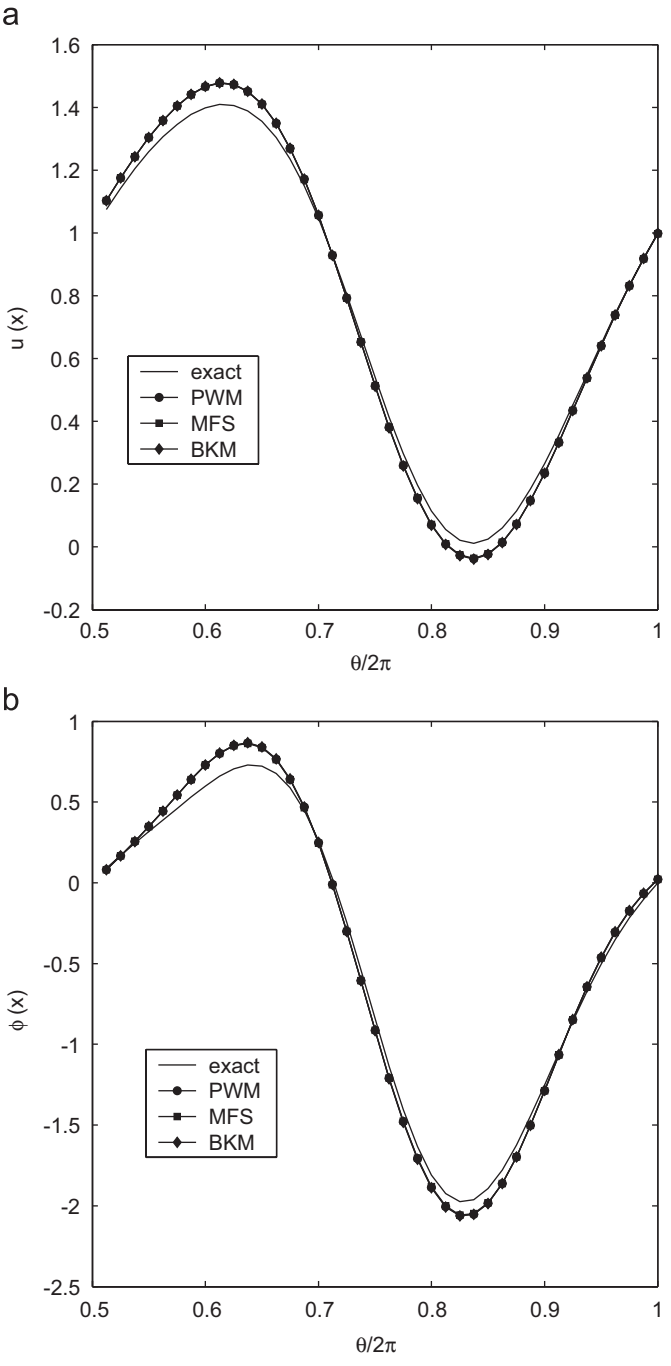

Fig. 11. The exact (—) and numerical (a) temperature $u(\mathbf{x})$, and (b) flux $\phi(\mathbf{x})$ on Γ_2, obtained using $n_s = 40$, $n = 40$, $\varepsilon = 3\%$ noise added into the Cauchy data and various meshless methods, namely the PWM (●), MFS (■) and BKM (◆), for Example 2.

numerical results much more accurate than the BKM, i.e. by two orders in magnitude. This remark is also consistent with the findings for forward problems, namely the PWM and MFS with large source radii yield similar results and they are usually more accurate than the BKM, see Alves and Valtchev [41].

The numerical boundary temperature $u(\mathbf{x})$ and flux $\phi(\mathbf{x})$, obtained using the PWM, MFS and BKM with 3% noisy Cauchy data, for Example 2 are displayed in Figs. 11(a) and (b), respectively. It can be seen from these figures that the numerical solutions are in reasonable agreement with the exact one. The difference between the numerical solutions is negligible and all the retrieved numerical results are practically identical. The accuracies for the numerical results corresponding to the aforementioned meshless schemes are comparable and are maintained at a small level comparable to the noise level, as shown in Table 2, where p is the regularization parameter.

To further explore the comparison of the PWM, MFS and BKM for solving inverse problems associated with

Please cite this article as: Jin B, Marin L. The plane wave method for inverse problems associated with Helmholtz-type equations. Eng Anal Bound Elem (2007), doi:10.1016/j.enganabound.2007.08.005

Table 2
The accuracy of the numerical boundary temperature, rel(ϕ), and flux, rel(ϕ), obtained using the PWM, MFS and BKM, and $\varepsilon = 3\%$ noise added into the Cauchy data, for the inverse problem associated with Example 2

Method	Cond(**A**)	p	rel(u)	rel(ϕ)
PWM	1.043×10^{18}	8	4.378×10^{-2}	7.193×10^{-2}
MFS	5.378×10^{17}	8	4.324×10^{-2}	7.088×10^{-2}
BKM	1.918×10^{18}	8	4.437×10^{-2}	7.326×10^{-2}

Helmholtz-type equations, we test these schemes for a more challenging problem, i.e. Example 3 with $n = n_s = 100$, $\varepsilon = 3\%$ noise added into the Cauchy data and $\kappa = 8$, which is representative for medium wave numbers, see Shu and Xue [52]. The corresponding exact and numerical solutions for the boundary temperature and flux are displayed in Fig. 12. Taking into account the severe ill-posed nature of the inverse problem and challenges posed by the high wave number, see Shu and Xue [52], the results presented here are quite satisfactory. The PWM- and MFS-based results are practically identical, but they are slightly less accurate than those obtained using the BKM, also see Table 3. Therefore, we may conclude that the proposed scheme is comparable with the MFS and BKM in terms of accuracy.

For two-dimensional problems, forming the interpolation matrix **A** for the MFS and the BKM requires the evaluation of Bessel and modified Bessel functions and these are much more costly than evaluating the exponential functions for the PWM. Numerically, it was found that the computational time required for calculating the system matrix **A** for the PWM is approximately one seventh of that corresponding to the MFS or BKM. Therefore, the present meshless method is slightly superior to the MFS and BKM in terms of computational efficiency. The difference in computational efficiency could be very important for large-scale problems which may involve thousands of unknowns. However, for three-dimensional problems the computational efficiency is almost the same since the computation of the Bessel and modified Bessel functions reduces to that of trigonometric and exponential functions.

4.5. Stability analysis

The exact and numerical results for the temperature and flux on the under-specified boundary Γ_2, obtained using various levels of noise added into the Cauchy data, namely $\varepsilon \in \{0, 1, 2\}$, for Example 4 are presented in Figs. 13(a) and (b), respectively. It can be seen from these figures that the numerical solutions for the boundary temperature and flux represent very good approximations for their analytical values. Furthermore, from Figs. 13(a) and (b) it can be concluded that the numerical solutions for the temperature $u(\mathbf{x})$ and flux $\phi(\mathbf{x})$ on the under-specified boundary Γ_2, converge to and approximate their corresponding exact solutions better as the amount of noise in the data

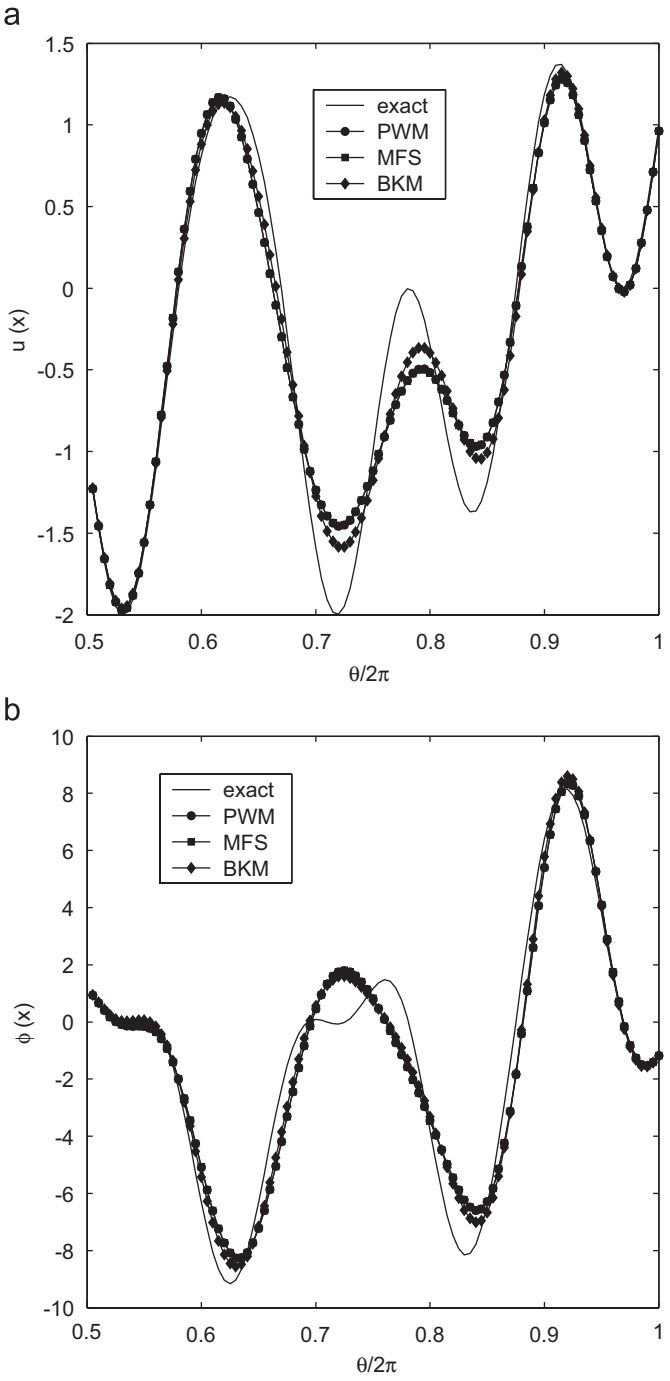

Fig. 12. The exact (—) and numerical (a) temperature $u(\mathbf{x})$, and (b) flux $\phi(\mathbf{x})$, on Γ_2, obtained using $n_s = 100$, $n = 100$, $\varepsilon = 3\%$ noise added into the Cauchy data and various meshless methods, namely the PWM (•), MFS (■) and BKM (◆), for Example 3.

Table 3
The accuracy of the numerical temperature, rel(ϕ), and flux, rel(ϕ), obtained using the PWM, MFS and BKM, and $\varepsilon = 3\%$ noise added into the Cauchy data, for the inverse problem associated with Example 3

Method	Cond(**A**)	p	rel(u)	rel(ϕ)
PWM	1.278×10^{18}	23	2.278×10^{-1}	2.368×10^{-1}
MFS	2.850×10^{17}	23	2.286×10^{-1}	2.374×10^{-1}
BKM	2.224×10^{18}	23	1.887×10^{-1}	2.063×10^{-1}

Please cite this article as: Jin B, Marin L. The plane wave method for inverse problems associated with Helmholtz-type equations. Eng Anal Bound Elem (2007), doi:10.1016/j.enganabound.2007.08.005

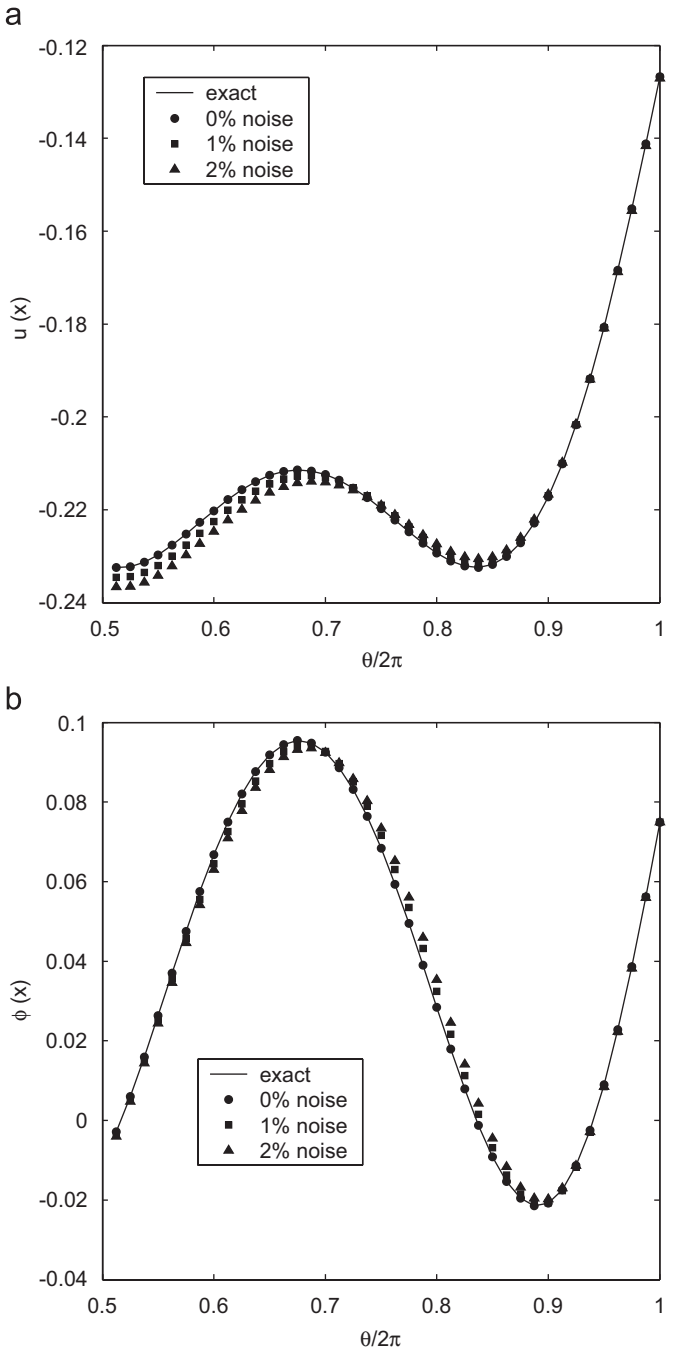

Fig. 13. The exact (—) and numerical (a) temperature $u(\mathbf{x})$, and (b) flux $\phi(\mathbf{x})$ on Γ_2, obtained using the PWM and various levels of noise added into the Cauchy data, namely $\varepsilon = 0\%$ (•), $\varepsilon = 1\%$ (■) and $\varepsilon = 2\%$ (▲), for Example 4.

decreases, while at the same time remaining stable. The accuracy of the numerical solutions for the level of noise $\varepsilon = 2\%$ is also tabulated in Table 4. It can be seen from this table that the error in the numerical solution is maintained at a small and comparable level with that in the boundary data.

So far, we have investigated the performance of the PWM + TSVD only for inverse problems in a smooth geometry. In fact, the proposed method works equally well

Table 4
The accuracy of the numerical temperature, rel(ϕ), and flux, rel(ϕ), obtained using the PWM and $\varepsilon = 2\%$ noise added into the Cauchy data, for the inverse problems associated with Examples 4–7

Example	Cond(**A**)	p	rel(u)	rel(ϕ)
4	2.078×10^{17}	8	1.235×10^{-2}	6.467×10^{-2}
5	9.336×10^{17}	10	7.157×10^{-3}	5.546×10^{-2}
6	5.203×10^{19}	29	5.365×10^{-3}	1.837×10^{-2}
7	9.149×10^{17}	8	7.654×10^{-2}	9.659×10^{-2}

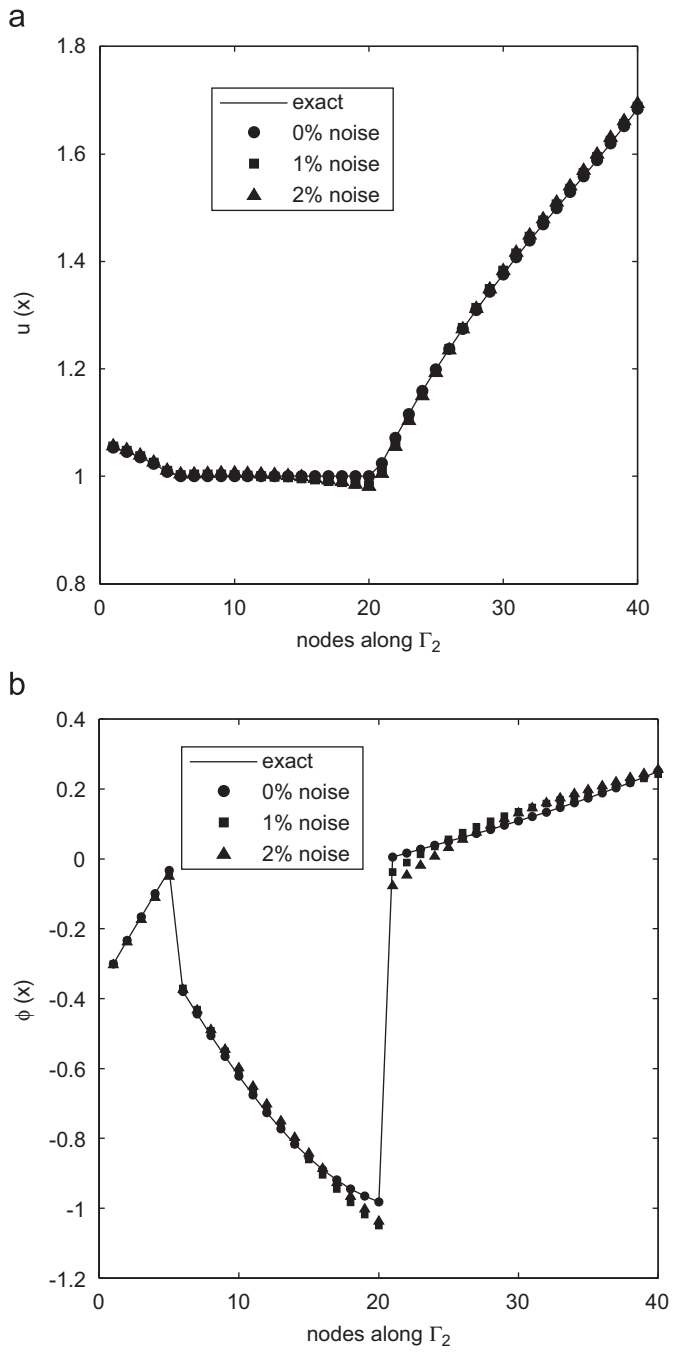

Fig. 14. The exact (—) and numerical (a) temperature $u(\mathbf{x})$, and (b) flux $\phi(\mathbf{x})$ on Γ_2, obtained using the PWM and various levels of noise added into the Cauchy data, namely $\varepsilon = 0\%$ (•), $\varepsilon = 1\%$ (■) and $\varepsilon = 2\%$ (▲), for Example 5.

Please cite this article as: Jin B, Marin L. The plane wave method for inverse problems associated with Helmholtz-type equations. Eng Anal Bound Elem (2007), doi:10.1016/j.enganabound.2007.08.005

for inverse problems in a non-smooth geometry. To illustrate this, we consider the inverse problem in the piecewise smooth geometry, as given by Example 5. The numerical results for Example 5 are presented in Figs. 14(a) and (b). With up to 2% noise in the boundary data, the numerical results are found to be in good agreement with their corresponding exact solutions. The accuracy of the numerical results achieved in this case is comparable with that obtained for inverse problems in a smooth geometry, as indicated in Table 4. These results show clearly the strength of the present scheme for problems with complicated geometry. Note that the solution is smooth in spite of the nonsmooth geometry considered and this is usually necessary to guarantee the fast convergence of the PWM, as in the case of the MFS and BKM, see Golberg and Chen [32] and Hon and Chen [34]. For problems with singular solutions, such as those caused by re-entrant corners and/or boundary conditions, a special treatment is required. The most popular technique is to approximate the solution by the leading terms of the local expansion of the solution around the singularity and to enforce the boundary conditions by means of Lagrange multipliers or penalty methods etc., see Karageorghis [53] and Li et al. [54].

The proposed scheme can be extended to three-dimensional problems in a straightforward manner. The exact and numerical results for the temperature $u(\mathbf{x})$ and the flux $\phi(\mathbf{x})$ on the surface $\{(x_1, x_2, 0.5)| -0.5 < x_1, x_2 < 0.5\} \subset \Gamma_2$, obtained with $\varepsilon = 2\%$ noise added into the Cauchy data, for the three-dimensional modified Helmholtz equation as given by Example 6, are shown in Figs. 15(a) and (b), respectively, while their corresponding error distributions are illustrated in Figs. 15(c) and (d), respectively. It can be

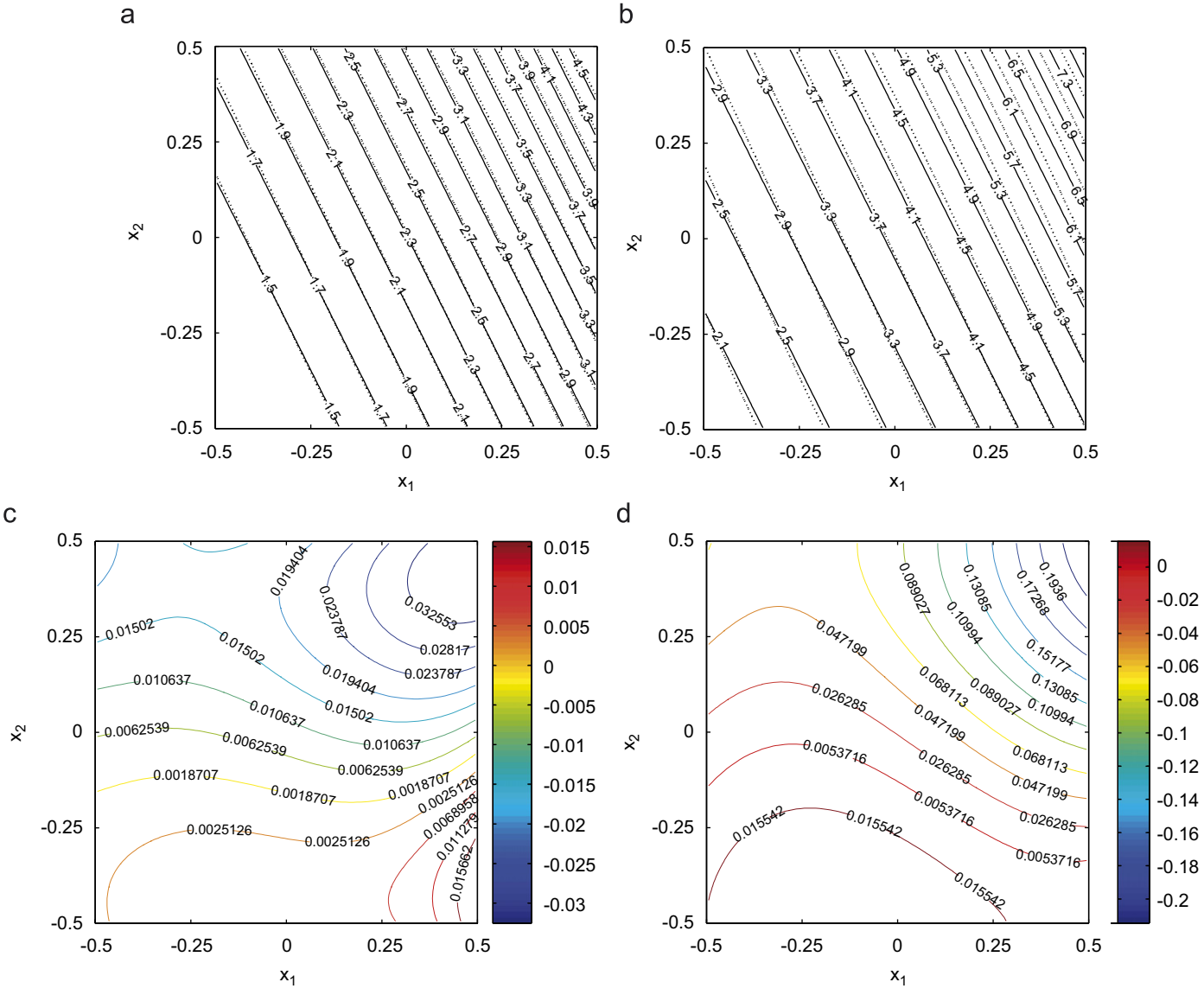

Fig. 15. The exact (—) and numerical (···) (a) temperature $u(\mathbf{x})$, and (b) flux $\phi(\mathbf{x})$, and the error distribution corresponding to (c) $u(\mathbf{x})$, and (d) $\phi(\mathbf{x})$, on the surface $\{(x_1, x_2, 0.5)| -0.5 < x_1, x_2 < 0.5\}$, obtained using the PWM and $\varepsilon = 2\%$ noise added into the Cauchy data, for Example 6.

Please cite this article as: Jin B, Marin L. The plane wave method for inverse problems associated with Helmholtz-type equations. Eng Anal Bound Elem (2007), doi:10.1016/j.enganabound.2007.08.005

seen from these figures that the numerical results reconstructed for $u(\mathbf{x})$ and $\phi(\mathbf{x})$ on the boundary Γ_2 are in good agreement with their corresponding exact solutions. From Fig. 15 we can conclude that the PWM + TSVD is also applicable to three-dimensional inverse problems. This is important especially for problems with a complicated geometry since generating a good quality mesh for a complicated geometry in higher dimensions could be costly.

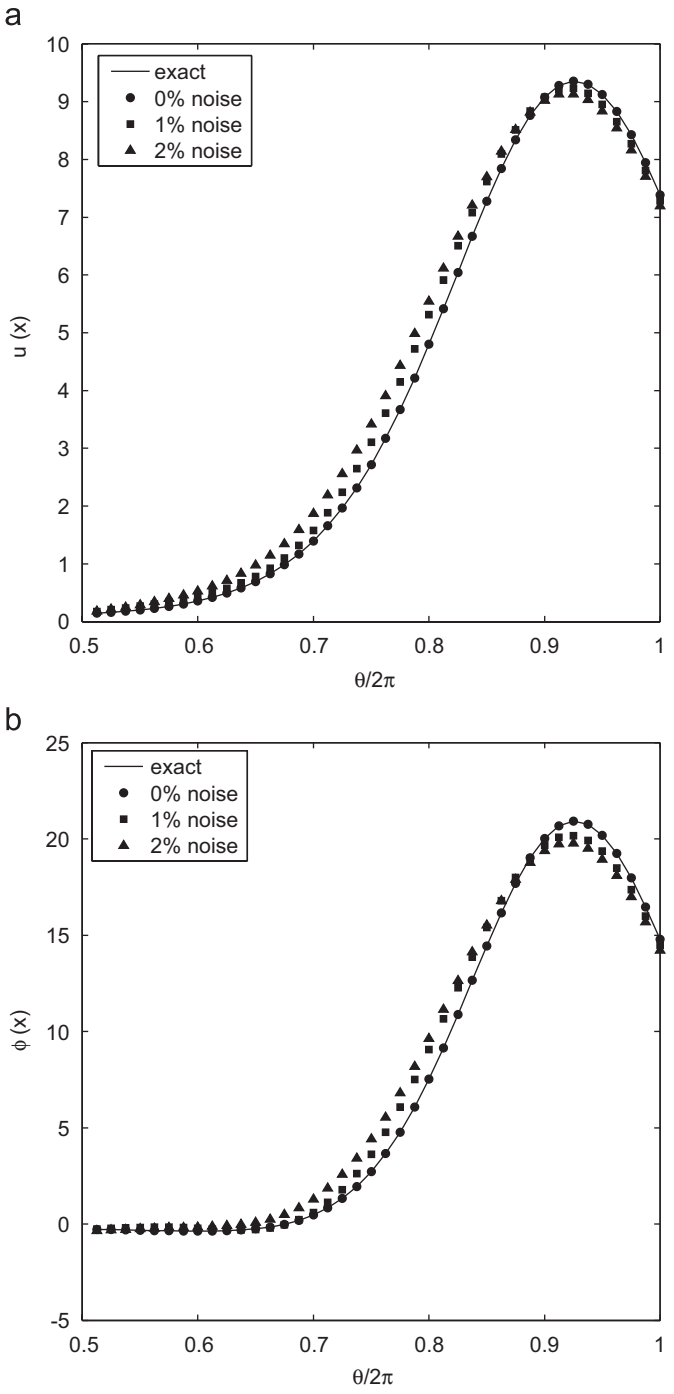

Fig. 16. The exact (—) and numerical (a) temperature $u(\mathbf{x})$, and (b) flux $\phi(\mathbf{x})$ on Γ_2, obtained using the PWM and various levels of noise added into the boundary and internal data, namely $\varepsilon = 0\%$(●), $\varepsilon = 1\%$ (■) and $\varepsilon = 2\%$ (▲), for Example 7.

The present numerical method works equally well for inverse boundary value problems with internal measurements. To illustrate this point, we consider the inverse problem for the two-dimensional modified Helmholtz equation corresponding to Example 7, where the internal measurement points are scattered in the domain as shown in Fig. 1(b). The numerical results for Example 7, obtained with various levels of noise added into the boundary and internal data, are presented in Fig. 16. From this figure, as well as Table 4, it can be seen that an excellent agreement between the numerical and analytical solutions is attained for all the levels of noise considered. This is clearly advantageous over traditional methods, which can only handle cumbersomely problems involving scattered internal measurements. Although not presented herein, it should be mentioned that similar results have been obtained for three-dimensional inverse boundary value problems for Helmholtz-type equations with internal measurements.

Overall, from Figs. 13–16 and Table 4, we can conclude that the proposed numerical scheme is stable with respect to decreasing the amount of noise, as well as versatile for complicated domains. Moreover, the solution and its high-order derivatives in the domain are readily available by direct differentiation.

5. Conclusions

In this paper, a meshless method for solving inverse boundary value problem associated with Helmholtz-type equations has been developed. The equation was discretized using the PWM, whilst the ill-conditioning of the resulting system of linear algebraic equations was overcome by the TSVD, in conjunction with the L-curve criterion. The numerical results for two- and three-dimensional problems indicate that for both smooth and piecewise smooth geometries accurate, convergent and stable numerical solutions can be obtained. The comparative study presented in Section 4.4 has shown that the PWM is also competitive with other meshless methods used for solving numerically inverse problems associated with Helmholtz-type equations.

There are several potential extensions of the present scheme, which are currently under investigation. Firstly, a much wider class of inhomogeneous problems can be conveniently handled using the proposed method with simple and minor modifications when combined with techniques for obtaining a particular solution, such as the dual reciprocity and multiple reciprocity methods. Secondly, the present algorithm can be extended in a straightforward manner to convection–diffusion problems and problems in anisotropic media. For details on this aspect, we refer the reader to Appendix A. Finally, the recent algorithmic innovations of the PWM by the scaling method, see Vergini and Saraceno [55] and Barnett et al.

Please cite this article as: Jin B, Marin L. The plane wave method for inverse problems associated with Helmholtz-type equations. Eng Anal Bound Elem (2007), doi:10.1016/j.enganabound.2007.08.005

[56], may provide the essential means for its successful application to problems with very high wave numbers.

Acknowledgements

The authors would like to thank Professor Vladimir Kozlov for his kind provision of relevant literature, as well as the reviewers for their constructive comments.

Appendix A. Plane waves for anisotropic problems

In this section, we derive the plane waves for the Helmholtz, modified Helmholtz and convection–diffusion equations in anisotropic media. These plane waves may be employed to solve relevant forward and inverse problems.

Firstly, we consider the Helmholtz equation in an anisotropic medium, namely

$$\nabla \cdot (\mathbf{K}\nabla u) + \kappa^2 u = 0, \quad \mathbf{x} \in \Omega, \tag{31}$$

where the constant second order tensor $\mathbf{K} = [k_{lm}]$ is symmetric and positive definite, and thus it admits the Cholesky factorization [51]

$$\mathbf{K} = \mathbf{L}\mathbf{L}^{\mathrm{T}}, \tag{32}$$

where $\mathbf{L}$ is a lower-triangular matrix. We define the following plane wave:

$$u^*(\mathbf{x}, \mathbf{d}) = \mathrm{e}^{\mathrm{i}\kappa \mathbf{d}^{\mathrm{T}}\mathbf{L}^{-1}\mathbf{x}}. \tag{33}$$

Then it is easy to verify that

$$\nabla u^* = \mathrm{i}\kappa u^* \mathbf{L}^{-\mathrm{T}}\mathbf{d} \tag{34}$$

and

$$\begin{aligned}\nabla \cdot (\mathbf{K}\nabla u^*) &= \nabla \cdot (\mathrm{i}\kappa u^* \mathbf{K}\mathbf{L}^{-\mathrm{T}}\mathbf{d}) = \mathrm{i}\kappa \nabla u^* \cdot (\mathbf{K}\mathbf{L}^{-\mathrm{T}}\mathbf{d}) \\ &= -\kappa^2 \mathbf{d}^{\mathrm{T}}\mathbf{L}^{-1}\mathbf{K}\mathbf{L}^{-\mathrm{T}}\mathbf{d}u^* = -\kappa^2 u^*,\end{aligned}$$

where we have made use of the identity $\mathbf{L}^{-1}\mathbf{K}\mathbf{L}^{-\mathrm{T}} = \mathbf{I}$, $\mathbf{I}$ being the identity matrix. Therefore, the plane wave given by Eq. (33) satisfies Eq. (31).

Next, we consider the modified Helmholtz equation in an anisotropic medium

$$\nabla \cdot (\mathbf{K}\nabla u) - \lambda^2 u = 0. \tag{35}$$

Analogous derivations show that its plane wave is given by

$$u^*(\mathbf{x}, \mathbf{d}) = \mathrm{e}^{\lambda \mathbf{d}^{\mathrm{T}}\mathbf{L}^{-1}\mathbf{x}}. \tag{36}$$

Finally, we consider the convection–diffusion equation in an anisotropic medium, namely

$$\nabla \cdot (\mathbf{K}\nabla u) + \mathbf{v} \cdot \nabla u - \eta^2 u = 0, \tag{37}$$

where $\eta \in \mathbb{R}$ and $\mathbf{v}$ is the velocity vector, and we let

$$v(\mathbf{x}) = \exp\left(\frac{\mathbf{v}^{\mathrm{T}}\mathbf{K}^{-1}\mathbf{x}}{2}\right) u(\mathbf{x}). \tag{38}$$

Then the function $v(\mathbf{x})$ satisfies

$$\nabla \cdot (\mathbf{K}\nabla v) - \mu^2 v = 0, \tag{39}$$

where the constant $\mu > 0$ is given by

$$\mu^2 = \eta^2 + \frac{\mathbf{v}^{\mathrm{T}}\mathbf{K}^{-1}\mathbf{v}}{4}. \tag{40}$$

Therefore, the plane wave for the convection–diffusion equation is given by

$$u^*(\mathbf{x}, \mathbf{d}) = \exp\left(-\frac{\mathbf{v}^{\mathrm{T}}\mathbf{K}^{-1}\mathbf{x}}{2} + \mu \mathbf{d}^{\mathrm{T}}\mathbf{L}^{-1}\mathbf{x}\right). \tag{41}$$

References

[1] Wood AS, Tupholme GE, Bhatti MIH, Heggs PJ. Steady-state heat transfer through extended plane surfaces. Int Commun Heat Mass Transfer 1995;22:99–109.
[2] Lax PD, Phillips RS. Scattering theory. New York: Academic Press; 1967.
[3] Jones DS. Methods in electromagnetic wave propagation. New York: Oxford University Press; 1979.
[4] Colton D, Kress R. Integral equation methods in scattering theory. New York: Wiley; 1983.
[5] Chen JT. Recent development of dual BEM in acoustic problems. Comput Methods Appl Mech Eng 2000;188:833–45.
[6] Pike ER, Sabatier P, editors. Scattering. London: Academic Press; 2001.
[7] Harari I. A survey of finite element methods for time-harmonic acoustics. Comput Methods Appl Mech Eng 2006;195:1594–607.
[8] John F. Continuous dependence on data for solutions of partial differential equations with a prescribed bound. Commun Pure Appl Math 1960;13:551–85.
[9] Hrycak T, Isakov V. Increased stability in the continuation of solutions to the Helmholtz equation. Inverse Prob 2004;20:697–712.
[10] Reginska T, Reginska K. Approximate solution of a Cauchy problem for the Helmholtz equation. Inverse Probl 2006;22:975–89.
[11] Knightly GH, St. Mary DF. Stable marching schemes based on elliptic models of wave propagation. J Acoust Soc Am 1993;93:1866–72.
[12] Bai MR. Application of BEM-based acoustic holography to radiation analysis of sound sources with arbitrarily shaped geometries. J Acoust Soc Am 1992;92:533–49.
[13] Wang Z, Wu SF. Helmholtz equation least-squares method for reconstructing the acoustic pressure field. J Acoust Soc Am 1997;102:2020–32.
[14] Wu SF, Yu J. Reconstructing interior acoustic pressure fields via Helmholtz equation-least-squares method. J Acoust Soc Am 1998;104:2054–60.
[15] Isakov V, Wu SF. On theory and application of the Helmholtz equation least squares method in inverse acoustics. Inverse Probl 2002;18:1147–59.
[16] Semenova T, Wu SF. On the choice of expansion functions in the Helmholtz equation least-squares method. J Acoust Soc Am 2005;117:701–10.
[17] DeLillo T, Isakov V, Valdivia N, Wang L. The detection of the source of acoustical noise in two dimensions. SIAM J Appl Math 2001;61:2104–21.
[18] Natterer F, Wübbeling F. A propagation–backpropagation method for ultrasound tomography. Inverse Probl 1995;11:1225–32.
[19] Natterer F, Wübbeling F. Marching schemes for inverse acoustic scattering problems. Numer Math 2005;100:697–710.
[20] Jin B, Zheng Y. Boundary knot method for some inverse problems associated with the Helmholtz equation. Int J Numer Methods Eng 2005;62:1636–51.
[21] Jin B, Zheng Y. A meshless method for some inverse problems associated with the Helmholtz equation. Comput Methods Appl Mech Eng 2006;195:2270–88.

Please cite this article as: Jin B, Marin L. The plane wave method for inverse problems associated with Helmholtz-type equations. Eng Anal Bound Elem (2007), doi:10.1016/j.enganabound.2007.08.005

[22] Marin L, Lesnic D. The method of fundamental solutions for the Cauchy problem associated with two-dimensional Helmholtz-type equations. Comput Struct 2005;83:267–78.
[23] Marin L. A meshless method for the numerical solution of the Cauchy problem associated with three-dimensional Helmholtz-type equations. Appl Math Comput 2005;165:355–74.
[24] Wei T, Hon YC, Ling L. Method of fundamental solutions with regularization techniques for Cauchy problems of elliptic operators. Eng Anal Boundary Elem 2007;31:373–85.
[25] Marin L, Elliott L, Heggs PJ, Ingham DB, Lesnic D, Wen X. An alternating iterative algorithm for the Cauchy problem associated to the Helmholtz equation. Comput Methods Appl Mech Eng 2003;192:709–22.
[26] Marin L, Elliott L, Heggs PJ, Ingham DB, Lesnic D, Wen X. Conjugate gradient-boundary element solution to the Cauchy problem for Helmholtz-type equations. Comput Mech 2003;31:367–77.
[27] Marin L, Elliott L, Heggs PJ, Ingham DB, Lesnic D, Wen X. Comparison of regularization methods for solving the Cauchy problem associated with the Helmholtz equation. Int J Numer Methods Eng 2004;60:1933–47.
[28] Kozlov VA, Mazỳa VG, Fomin AV. An iterative method for solving the Cauchy problem for elliptic equations. USSR Comput Math Math Phys 1992;31:45–52.
[29] Griebel M, Schweitzer MA, editors. Meshfree methods for partial differential equations. Berlin, New York: Springer; 2003.
[30] Liu GR. Meshfree methods: Moving beyond the finite element method. Boca Raton, FL: CRC Press; 2003.
[31] Fairweather G, Karageorghis A. The method of fundamental solutions for elliptic boundary value problems. Adv Comput Math 1998;9:69–95.
[32] Golberg MA, Chen CS. The method of fundamental solution for potential Helmholtz and diffusion problems. In: Golberg MA, editor. Boundary integral methods—numerical and mathematical aspects. Southampton: Computational Mechanics Publications; 1998. p. 103–76.
[33] Chen W, Tanaka M. A meshless, integration-free, and boundary-only RBF technique. Comput Math Appl 2002;43:379–91.
[34] Hon YC, Chen W. Boundary knot method for 2D and 3D Helmholtz and convection–diffusion problems under complicated geometry. Int J Numer Methods Eng 2003;56:1931–48.
[35] Pinkus A. Approximating by ridge functions. In: Le Mehaute A, Rabut C, Schumaker LL, editors. Surface fitting and multiresolution methods. Nashville, TN: Vanderbilt University Press; 1997. p. 279–92.
[36] John F. Plane waves and spherical means applied to partial differential equations. New York: Interscience Publishers; 1955.
[37] Heller EJ. Bound-state eigenfunctions of classically chaotic Hamiltonian systems: Scars of periodic orbits. Phys Rev Lett 1984;53:1515–8.
[38] Li B, Robnik M, Hu B. Relevance of chaos in numerical solutions of quantum billiards. Phys Rev E 1998;57:4095–105.
[39] Sakoda K. Numerical analysis of the interference patterns in the optical transmission spectra of a square photonic lattice. J Opt Soc Am B 1997;14:1961–6.
[40] Alves CJS, Valtchev SS. Numerical simulation of acoustic wave scattering using a meshfree plane waves method. In: International Workshop on Meshfree Methods 2003, URL: ⟨http://www.math.ist.utl.pt/meshfree/svilen.pdf⟩; 2003.
[41] Alves CJS, Valtchev SS. Numerical comparison of two meshfree methods for acoustic wave scattering. Eng Anal Boundary Elem 2005;29:371–82.
[42] Li X. On solving boundary value problems of modified Helmholtz equations by plane wave functions. J Comput Appl Math 2006;195:66–82.
[43] Abramowitz M, Stegun IA, editors. Handbook of mathematical functions, with formulas, graphs, and mathematical tables. New York: Dover; 1965.
[44] Kroó A. On approximation by ridge functions. Constr Approximation 1997;13:447–60.
[45] Barron AR. Universal approximation bounds for superposition of a sigmoidal function. IEEE Trans Inform Theory 1993;39:930–45.
[46] Petrushev PP. Approximation by ridge functions and neural networks. SIAM J Math Anal 1998;30:155–80.
[47] Hansen PC. Rank-deficient and discrete ill-posed problems: Numerical aspects of linear inversion. Philadelphia: SIAM; 1998.
[48] Hansen PC, O'Leary DP. The use of the *L*-curve in the regularization of discrete ill-posed problems. SIAM J Sci Comput 1993;14:1487–503.
[49] Ling L. Matlab program pointonsphere.m., URL: ⟨http://www.mathworks.com/matlabcentral⟩.
[50] Galperin EA, Zheng Q. Solution and control of PDE via global optimization methods. Comput Math Appl 1993;25:103–18.
[51] Golub GH, Van Loan CF, Matrix computations. 3rd ed. Baltimore: Johns Hopkins University Press; 1996.
[52] Shu C, Xue H. Solution of Helmholtz equation by differential quadrature method. Comput Methods Appl Mech Eng 1999;175:203–12.
[53] Karageorghis A. Modified methods of fundamental solutions for harmonic and biharmonic problems with boundary singularities. Numer Methods Partial Differential Equations 1992;8:1–19.
[54] Li ZC, Lu TT, Hu HY, Cheng AH-D. Trefftz and collocation methods. Southampton: WIT Press; 2005.
[55] Vergini E, Saraceno M. Calculation by scaling of highly excited states of billiards. Phys Rev E 1995;52:2204–7.
[56] Barnett AH, Cohen D, Heller EJ. Deformations and dilations of chaotic billiards, dissipation rate, and quasi-orthogonality of the boundary wavefunctions. Phys Rev Lett 2000;85:1412–5.

Please cite this article as: Jin B, Marin L. The plane wave method for inverse problems associated with Helmholtz-type equations. Eng Anal Bound Elem (2007), doi:10.1016/j.enganabound.2007.08.005